Chapter 16

Guided Mode Studies of Liquid Crystal Layers

Fuzi Yang

Liquid Crystal Research Centre, Chemistry Department, Tsinghua University, Beijing 100084, China.

J. R. Sambles

Thin Film Photonics, School of Physics, University of Exeter, Exeter, EX4 4QL, UK.

16.1. Introduction

Although the liquid crystalline state of matter has been recognised for over 100 years [1,2] the explosive growth in the application of such materials as primary components in flat panel displays having low power consumption and compact dimensions has occurred only during the last 30 years. The worldwide demand for flat panel displays is huge and continues to drive further scientific investigations in liquid crystal (LC) science and technology. This has resulted in developments in materials synthesis giving rise to novel materials and new discoveries in the fundamental science of liquid crystal phases. In addition there has been substantial new device structure development strongly pushed by requirements from the display market.

Liquid crystals have the ability to flow while displaying anisotropic properties. They respond to (realign in) externally applied electric (or magnetic) fields. It is this response, coupled with the optical anisotropy, which has led to applications in flat panel display technology, including alpha/numeric displays, high resolution TV, data projection systems and monitors for desk and laptop computers etc. They also change their behaviour quite markedly with temperature and they are readily aligned by molecular scale surface structures. Consequently LC materials are also being used as sensors for temperature, stress and flow etc. For many of these applications, especially for displays, the optical behaviour of liquid crystals is vitally important and the optical response of a given LC geometry to changing conditions is a major issue. It may, for example, be important to know how some parameters of a liquid crystal, such as refractive index, dielectric permittivity, viscosity and elasticity coefficients etc., change with temperature, or how the apparent optical response of a thin LC layer changes under application of a field. From both a fundamental and a device perspective we may wish to investigate how the response of LC layers vary with surface treatment, the specifics of the cell geometry, or the elastic and/or viscous properties of the material. Knowledge of the form of the LC director profile in cells and subsequently its change with applied field is essential for developing a full understanding of device function from which further devices and applications may arise. For example for fast devices details of the electroclinic coefficients may be required, or viscosities may be needed. This may demand determining both the static and dynamic director response. In order to characterise fully the optical properties of a given liquid crystal, in a given cell geometry, with defined thickness and boundary treatments it is obvious that some form of appropriate structural study needs to be undertaken.

In many liquid crystal research laboratories the most common method used to explore the optical structure within a LC cell is that of polarised microscopy [3]. This provides a quick and simple procedure for exploring the approximate director profile allowing the study of cell uniformity, defect structures, phase transitions, the influence of aligning layers and also gives much of information on voltage controlled switching processes. However, by its very nature, polarised microscopy is an integral technique, which, through the transmitted intensity, provides an integrated optical response through the cell as a whole. Thus it cannot readily be used to resolve details of the director profile through the cell thickness or its variation with time during switching.

A second procedure, often used for the study of liquid crystals structures, even with thin cells (<10 μm), is X-ray scattering [4]. In bulk materials the X-ray scattering gives the symmetry of the phase and in thin layers it is primarily used to explore only the density wave layering found in S_A, S_C, S_C^* and other more ordered phases, for example in the study of ferroelectric LC materials [4]. This method may then give very useful information on the elastic deformation of the density wave, the layers, but it says almost nothing directly as regards the optical properties of the LC cell, which are vitally important for display applications.

At the same time as new display technologies using liquid crystalline materials were being developed in the early 1970s, new optical techniques were being introduced in the broad area of light guiding. This is particularly obvious in the area of optical fibre communications. Accompanying this development of optical fibre technology light guiding in thin films and layered structures has also received considerable attention both for integrated optics and other applications. During these developments a new optical probing technique, the guided mode technique [5,6], for investigating the optical index profiles in guiding structures has materialised. This technique utilises the fact that a series of discrete (quantised waveguide momentum) modes may be excited in thin films or fibres, their mode spectrum being dependent upon the refractive index distribution in, and the dimensions of, the structure. By exploring in depth the guided mode spectrum it is possible to characterise in some detail the optical properties of thin films or fibre guides. At the heart of LC displays are liquid crystals in the form of a thin layer, with a thickness of the order of a few microns with a director structure which varies little laterally, but may vary substantially through the cell. This layer is sandwiched between two glass plates (the two cell walls) which have some transparent conductive coatings (e.g. ITO) and liquid crystal alignment layers on them. Thus although most liquid crystal display structures are not designed as optical waveguides they often are just that, albeit rather 'leaky' ones. So in parallel with the development of new liquid crystal devices we have seen the evolution of a range of optical waveguide characterization techniques which allow the probing of the details of the director structure in these devices. It is these new techniques which are the primary focus of this chapter and which will be discussed later in detail.

In the early 70s, both guided wave optics (often narrowly labelled integrated optics) and liquid crystal studies were in their infancy and, based upon the material syntheses and the requirements of display devices, much work centred simply on optical microscopy of the nematic mesophase of liquid crystals. Theoretical modelling of the nematic phase was developed quite early and the director profile in waveguides made of such nematics is quite simple, even in the case of finite surface tilt and twist in the cell. Because of this, even though the optical guided mode technique has great potential as a tool for studying both physical and chemical processes in thin films [7] there have been few such investigations of nematic liquid crystal cells. Thus in addition to polarised microscopy only the monitoring of the transmitted intensity for normal incidence light together with modelling the optical response of liquid crystal cells based upon 2×2 Jones' matrix are used as standard procedures in most liquid crystal research laboratories. Often liquid crystal 'waveguides' are used as devices, as displays, in modulators [8,9], switches [10] or deflectors [11] but with limited studies of details of the optical tensor distribution in cells except for a few measurements of refractive indices and surface pre-tilt angle.

However, several new areas of liquid crystal research have led to the guided mode technique becoming more and more useful and important. Firstly, in the early 80s the prediction [12] and experimental observation [13] of the surface stabilised ferroelectric, S_C^*, liquid crystal (SSFLC) state introduced a challenge to unravel and understand the complex optical tensor profile in such LC cells. In view of the fact that thin cells containing S_C^* liquid crystals may have many applications in fast optical switching, displays and TV and also because currently, unlike in the nematic case, there is still not a convenient theoretical model, then the experimental unravelling of the director structures in such cells is vital. Secondly, even for some simpler phases, such as nematic or S_A phases, the director structure through the whole cell is not necessarily straightforward. For example there may exist coexisting nematic and S_A phases in a twisted liquid crystal cell [14] in which the director profile through the LC cell is stepped in several sections, which can only be found in detail by the guided mode techniques. Any other method, such as polarised microscopy or monitoring the transmission intensity from normal incidence, can not distinguish this stepped structure. Also from theoretical modelling and experimental demonstration the method based on monitoring the transmission intensity from normal incidence and 2×2 Jones' matrix which treats the LC cell as a simple slab may sometimes introduce serious errors in the measured parameters [15]. By

contrast the guided mode technique together with theoretical modelling based upon the 4×4 Berreman's matrix method, treating the LC cell as a real multi-layer optical system will give the correct results. Finally, in dynamic studies of liquid crystal films the director profile and its change with time and field are very complex. The serious profile degeneracy problems associated with the usual optical procedures may only be solved by use of the recently developed dynamic LC guided mode technique [16,17].

In this chapter we first introduce briefly the background of the optical guided mode technique, including the guided mode spectrum, the optical field distribution for different order modes and various optical coupling methods to couple the radiation into the waveguides. Then we illustrate four different types of liquid crystal waveguide geometry, including the fully-guided mode geometry, the fully-leaky mode geometry, the half-leaky guided mode geometry and the improved fully-leaky guided mode geometry. Finally we briefly discuss the dynamic LC guided mode technique. Various experimental results obtained recently using different types of LC optical guided mode techniques are presented to show the power of the techniques.

16.2 Optical Guided Waves [18]

16.2.1 Optical Waveguide Modes

To introduce the background to optical waveguides let us first consider the simplest geometry comprising a planar slab of perfectly transparent isotropic dielectric surrounded by semi-infinite blocks of perfectly transparent isotropic dielectric. The geometry is invariant in the plane normal to the page, i.e. the y-z plane as shown in Figure 16.1 <Figure 16.1>. The three materials in the waveguide geometry have been labelled as the cladding layer, of index n_c, the guiding layer, of index n_g and the substrate layer of index n_s. For full-waveguiding the situation of $n_g > n_s$ and $n_g > n_c$ is required. For the ensuing discussion we further suppose $n_s > n_c$, unless explicitly stated otherwise, so $n_g > n_s > n_c$.

A ray optics picture is first used here to describe the optical modes [5] propagating in the planar waveguide. The situation to be considered is that of a plane wave of radiation, with an incident angle β (angle between the wavefront normal and the normal to the boundary of the geometry) to the interface, propagating inside the guiding layer as shown in Figure 16.2 <Figure 16.2>. According to Snell's Law (basically conservation of momentum in the y-z plane) the critical angles at the top and bottom interfaces of the geometry are given by

$$\beta_c = \sin^{-1}\left(\frac{n_c}{n_g}\right) \tag{16.1}$$

and

$$\beta_s = \sin^{-1}\left(\frac{n_s}{n_g}\right) \tag{16.2}$$

where $\beta_s > \beta_c$. In Figure 16.2 there are three different zigzag pictures for different ranges of the internal angle β.

When $\beta_s < \beta < \pi/2$ the light is primarily contained inside the guiding layer by total internal reflection at both the top and bottom boundaries. According to the ray optics picture the light propagates along the zigzag path shown in Figure 16.2a. This case corresponds to a fully-guided mode. Even if the ray is totally inside the guiding layer, the optical radiation field is not entirely constrained to the slab since there are evanescently decaying fields present in both the substrate and cladding layers. However, if there are no imaginary parts to the refractive indices of the two layers the optical energy flow of the modes will be strictly along the z-direction and no radiation propagates away in either of the semi-infinite blocks.

Secondly when $\beta_c < \beta < \beta_s$, as shown in Figure 16.2b, only one interface, the cladding interface, acts as a totally reflecting surface, part of the radiation energy of the modes escapes into the substrate area. This situation corresponds to a substrate radiation mode, and it is obvious that the radiation energy rapidly leaks out of the guiding layer. This type of waveguide may be labelled as a half-leaky waveguide – it only leaks radiation into one half space of the geometry.

Finally for $\beta < \beta_c$ the radiation energy of the modes will leak into both the substrate and cladding half spaces across both interfaces as shown in Figure 16.2c. Thus this is labelled a fully-leaky waveguide and the confinement of radiation within the guided layer is quite weak.

In all three cases described above, but primarily in the first case of fully-guiding, since the light is propagating either entirely or partially in the guiding layer, then exploring modes excited in the geometry will give information on the optical properties of the guiding layer. Different order modes, which propagate with different momenta along the z-direction in the waveguide geometry, will have different numbers of optical field maxima across (in the x-direction) the guiding layer. Both the in-plane momentum and the optical field distribution of different order modes are dependent upon the thickness and refractive index profile of the guiding layer. Thus each mode will have a different sensitivity to particular portions of the guiding layer. This idea will be discussed later. For the moment the guiding condition, i.e. the reason for creating different order modes, will be explored in more detail.

For the fully guiding situation, even though the saw-tooth ray picture clearly gives a description of a mode with oblique-up and oblique-down beams, from the wave-nature of the light a sustainable mode propagating in the guiding layer is only one that does not destructively interfere with itself. Thus there will only be a few angles of propagation for the zigzag which give correct constructive interference, i.e. there can only be a finite set of waveguide modes for a given guiding geometry.

Let us consider only the component of momentum normal to the waveguide plane, that is in the x-direction. One might at first anticipate a very simple condition for constructive interference, that is

$$k_x = \frac{m\pi}{d} \tag{16.3}$$

where m is an integer and d is the thickness of the guiding layer. In the equation (16.3), however, the phase shifts at the top and bottom interfaces are ignored. Incorporating correctly the phase shifts ($-2\Phi_{gs}$) and ($-2\Phi_{gc}$) at the substrate and cladding interfaces A more general equation can be given as

$$2k_x d - 2\Phi_{gs} - 2\Phi_{gc} = 2m\pi \tag{16.4}$$

Of course k_x is simply given through the relationship

$$k_x = k_0 n_g \cos \beta \tag{16.5}$$

where k_0 is $2\pi / \lambda$ and λ is the light wavelength in free space.

If we join equations (16.4) and (16.5) together, then an even stricter and preferred form of the equation involving the waveguide momentum, k_z, can be given as

$$k_z = \left[k_0^2 n_g^2 - \left(\frac{m\pi + \Phi_{gs}(\beta) + \Phi_{gc}(\beta)}{d} \right)^2 \right]^{1/2} \tag{16.6}$$

where $2\Phi_{gs}$ and $2\Phi_{gc}$ are also functions of k_0 itself. This equation still gives a discrete set of guided modes but it is clearly not that trivial to solve. We will take this equation a stage further by replacing $\Phi_{gs}(\beta)$ and $\Phi_{gc}(\beta)$ by the appropriate functional forms found from Fresnel equations. According to the Fresnel equations it is clear that both $\Phi_{gs}(\beta)$ and $\Phi_{gc}(\beta)$ will be polarisation sensitive and it is generally the situation that there will be two families of discrete momentum modes, one set transverse electric (TE or s-polarised) and one set transverse magnetic (TM or p-polarised).

For the situation of both half-leaky and fully-leaky waveguides these standing wave mode solutions, excited at specific in-plane momenta, are no longer so well defined. In principle leaky modes exist for any momentum within the waveguide provided it is less than the cut-off momentum corresponding to the critical angle defined by β_s. Nevertheless, depending on the refractive index profile of the guiding layer, and the geometry of the waveguide, there will still be some selected in-plane momenta at which there are stronger optical fields confined in the guiding layer.

16.2.2 The Field Distributions of Optical Guided Modes [5,6]

In order to show how different order guided modes are sensitive to different spatial regions of a waveguide wave optics should be used and optical field profiles in a slab waveguide need to be explored. From Maxwell's electromagnetic theory the two important equations in isotropic (non-magnetic) lossless dielectrics are

$$\nabla \times \underline{\mathbf{E}}(\underline{\mathbf{r}}, t) = -\mu_0 \frac{\partial \underline{\mathbf{H}}(\underline{\mathbf{r}}, t)}{\partial t} \tag{16.7}$$

$$\nabla \times \underline{\mathbf{H}}(\underline{\mathbf{r}}, t) = \varepsilon_0 n^2 \frac{\partial \underline{\mathbf{E}}(\underline{\mathbf{r}}, t)}{\partial t} \tag{16.8}$$

where ε_0 and μ_0 are the dielectric permittivity and magnetic permeability of free space respectively and n is the refractive index of the dielectric.

When a plane wave propagates along the z-direction (Figure 16.1) with the propagation constant γ ($= k_z$) then the electromagnetic field may be expressed as

$$\underline{\mathbf{E}} = \underline{\mathbf{E}}(x, y)\exp[i(\varpi t - \gamma z)] \tag{16.9}$$

$$\underline{\mathbf{H}} = \underline{\mathbf{H}}(x, y)\exp[\mathbf{i}(\varpi t - \gamma z)] \tag{16.10}$$

which combined with (16.7) and (16.8). Being aware that $E_z = H_z = 0$, $\partial/\partial t \equiv i\omega$; $\partial/\partial z \equiv -i\gamma$; $\partial/\partial y = 0$, gives us two independent solutions of the form

$$\frac{\partial^2 \mathbf{E_y}}{\partial \mathbf{x}^2} + [k_0{}^2 n^2 - \gamma^2]\mathbf{E_y} = 0 \tag{16.11}$$

$$\frac{\partial^2 \mathbf{H_y}}{\partial \mathbf{x}^2} + [k_0{}^2 n^2 - \gamma^2]\mathbf{H_y} = 0 \tag{16.12}$$

These two equations are the solutions for transverse electric and transverse magnetic optical fields respectively.

To obtain the optical field distribution in the waveguide appropriate boundary conditions have to be imposed to give E_y and H_y as functions of x. The boundary conditions are conservation of tangential $\underline{E}$ and $\underline{H}$ and also conservation of normal $\underline{D}$ and $\underline{B}$. For the waveguide geometry mentioned above the fields are not zero in the surrounding media, they simply decay exponentially into these two regions. (This, in effect, is identical in form to the quantum machanical boundary conditions for a non-infinite potential well.) For the TE case E_y and $\partial E_y/\partial x$ are continuous across the boundary while for the TM case H_y and $\partial H_y/\partial x$ are continuous across the boundary. The phase shifts at the interfaces are introduced by these continuity conditions leading to the waveguide equation (16.4), where, as before, m is an integer running from 0, 1, etc., and of course the phase factors are different for TE and TM modes. In the TE case

$$\mathbf{\Phi_{gs}} = \tan^{-1}\left(\frac{\delta_s}{k_x}\right) \tag{16.13}$$

$$\mathbf{\Phi_{gc}} = \tan^{-1}\left(\frac{\delta_c}{k_x}\right) \tag{16.14}$$

and for the TM case

$$\mathbf{\Phi_{gs}} = \tan^{-1}\left[\left(\frac{n_g}{n_s}\right)^2 \frac{\delta_s}{k_x}\right] \tag{16.15}$$

$$\mathbf{\Phi_{gc}} = \tan^{-1}\left[\left(\frac{n_g}{n_c}\right)^2 \frac{\delta_c}{k_x}\right] \tag{16.16}$$

where

$$\delta_s = \left[\gamma^2 - k_0{}^2 n_s{}^2\right]^{1/2} \tag{16.17}$$

and

$$\delta_c = \left[\gamma^2 - k_0{}^2 n_c{}^2\right]^{1/2} \tag{16.18}$$

are the exponential decay coefficients for the evanescent fields in the substrate and cladding media respectively. From equations (16.17) and (16.18) it is clear that as γ continues to diminish (β continuously becoming smaller) δ_s and δ_c will become imaginary and one moves over to the 'leaky' situation. When $\gamma < k_0 n_s$ the situation becomes a continuous spectrum in γ rather than the discrete values found for the trapped modes. The various field profiles of the electromagnetic modes for different ranges of the propagation constant (in-plane momentum) are shown in Figure 16.3 <Figure 16.3> for the TE case. As expected it is clear that in the guided mode range the optical fields are concentrated in the guiding layer with evanescently decaying fields in the cladding and substrate areas. In the radiation mode range the optical fields of course propagate out into the cladding and substrate media. For the guided mode situation the field profiles produced from equations (16.11) and (16.12) for TE modes of order 0, 1 and 2 with the equivalent ray optics model are shown in Figure 16.4 <Figure 16.4>.

From equation (16.6) it is apparent that the fundamental mode, with m = 0, has the largest propagation constant γ (= k_z), close to the limit value of a plane wave in the guiding layer, $n_g k_0$. This mode, in the ray picture, has correspondingly the largest internal angle, β, close to $\pi/2$ and the longest 'wavelength' in the x-direction. For the TM modes the situation is much the same. The next order mode, with m = 1, has a smaller propagation constant than that of the mode m = 0 and will generally have zero optical field near to the centre of the guiding layer as shown in Figure 16.4. Thus it is clear that different order optical guided modes will have different field distributions through the guiding layer. As shown in Figure 16.4 the zero order mode will be much more sensitive to the centre of the guiding layer than would be the first order mode. Therefore it would be not difficult to see that this guided mode technique applied to the study of a liquid crystal layer having a complex director distribution through a cell may allow discrimination of details of the optical tensor varying through the layer. This information would be unobtainable by integral (polarised microscopy etc.) techniques.

According to the mode equation (16.4) it is also abundantly clear that the thicker the guiding layer the more modes it will support. In addition more modes can also be excited for shorter probing wavelengths of the incident light unless there is very strong optical dispersion of the guide indices with wavelength. Further details of optical waveguide theory and technology may be found in a range of review articles and books[5,6].

Up to now our discussion concerning optical waveguides has been limited to isotropic, lossless and uniform materials, however, in an optical waveguide having liquid crystals as the guiding layer it is highly unlikely that these assumptions will hold. Of the three assumptions that of low loss is generally not too worrying. If the losses are not too large, as in liquid crystals in the optical range, they only change the mathematics somewhat and make otherwise infinitely sharp modes available for excitation and detection. However, the non-uniformity is of fundamental interest and it is the anisotropy which most significantly affects the discussion thus far. These two points are briefly discussed in the following.

In general the eigenmodes of a waveguide geometry having an anisotropic guiding layer will not be pure TE or TM polarisations except for some special, high-symmetry structures. Thus the complex eigenmode solutions can not be readily be simply analysed using Maxwell equations, even though some methods based upon electromagnetic field theory have been developed [19] to try to solve this problem. Here we will explore a few situations which allow us to illustrate the behaviour of an anisotropic waveguide.

Let us restrict the discussion to just uniaxiality in the guiding layer itself. Consider a uniformly aligned uniaxial layer of liquid crystal as shown in Figure 16.5 <Figure 16.5> surrounded by semi-infinite cladding and substrate media with isotropic refractive indices n_c and n_s respectively. The liquid crystal is specified by indices parallel and perpendicular to the director, the optical axis **N**, n_e and n_o, respectively, and we assume $n_e > n_o$, i.e. the liquid crystal has positive anisotropy. For the general situation the director of the liquid crystal layer is tilted by θ from the x-axis and twisted by φ from the xoy plane as shown in Figure 16.5. The line AO is the wave-front normal for the eigenmode in the liquid crystal. One of the two semi-axes (OF and OB) of the ellipse, formed by the intersection of the plane perpendicular to the wave front AO and the index ellipsoid of the liquid crystal, gives the refractive index for this eigenmode propagating in the uniaxial layer. Firstly, choosing the very special case of the optic axis along the z-axis then, from Figure 16.5, it is simple to see that the TE guided modes depend only on n_o, while the TM eigenmodes depend on both n_e and n_o, with the lower order modes (with high β) depending mostly on n_o. Thus for this simple case the effective index for the TM eigenmodes changes with mode order. If now the optic axis is tilted so that it is still in the x-z-plane nothing fundamentally changes. The TE eigenmodes will still sense n_o while the TM eigenmodes sense a different combination of n_e and n_o. Secondly, if the optical axis lies instead along the x-axis, then the lowest order TM mode will sense n_e with the higher order modes becoming more sensitive to n_o. Of course all order TE modes will still sense n_o. In practice this means that when the optic axis is along the z-axis the TE and TM modes will have the same upper momentum limit, while for any other tilt of the optic axis in the x-z-plane the limit of the TM modes will, for $n_e > n_o$, move above the TE limit. Thirdly, if the optic axis lies along the y-axis, which is the simplest case for the optical axis lying out of the incidence plane xoz, now the TE modes are given by n_e while the TM modes are given by n_o, a very simple situation. For these three special cases mentioned above the eigenmodes propagating in an anisotropic waveguide geometry are pure TE or pure TM modes, even though their propagation constants may vary.

However, as soon as the optic axis is rotated out of the y-axis to some arbitrary angle in the x-y plane, or to some arbitrary angle in the y-z plane, or both, i.e. the opticl axis is at a general position in the frame as shown in Figure 16.5, the eigenmodes are no longer pure TE and TM. Thus an experimental investigation of such a system using radiation of a given linear polarisation, either TE or TM, will lead to polarisation conversion, the output radiation having some of the orthogonal polarisation component present. The signals from the polarisation conversion are very useful for investigating the director structure of liquid crystal waveguides since they are so clearly sensitive to both tilt and twist of the optical axis (the director) out of the plane of incidence of the exciting radiation.

Some analytical explanations can also be provided for the situation of polarisation conversion in the uniaxial guiding layer[20,21]. The geometry of Figure 16.5 gives

$$\cos\psi = \cos\theta\cos\beta - \sin\theta\sin\beta\sin\varphi \qquad (16.19)$$

where ψ is the angle between the optical axis (the director) and the wave-front normal of the eigenmode in the uniaxial layer. The index of the extraordinary eigenmode $n_e'(\beta_e)$ is defined by the semi-major axis OF of the ellipse formed by the

intersection of the plane perpendicular to the wave front AO and the index ellipsoid of the uniaxial layer. From Figure 16.5 this gives

$$n_e' = \frac{n_o n_e}{\sqrt{n_o^2 \sin^2\psi + n_e^2 \cos^2\psi}} \quad . \tag{16.20}$$

Of course the extraordinary eigenmode index lies within the range $n_e \geq n_e' \geq n_o$ and will correspond to a pure TE or a pure TM eigenmode for the three special situations mentioned above. In Figure 16.5, s-polarised radiation has its E field along the y-axis, whereas p-polarised radiation has its E field in the x-z plane. For either form of incident radiation, two eigenmodes are excited in the uniaxial layer, one with the E field along the short semi-axis OB in the ellipse BOF, and normal to the plane AO**N**, and a second with the E field along the major semi-axis OF in the ellipse BOF, and normal to OB. So the angle Ω between Oy and OB gives a measure of the s-to-p or p-to-s, conversion signal when either pure s or pure p radiation enters the uniaxial layer. From Figure 16.5 we obtain

$$\cos \mathbf{\Omega} = \frac{\sin\beta\cos\theta + \sin\theta\cos\beta\sin\varphi}{\sqrt{1 - (\cos\theta\cos\beta - \sin\theta\sin\beta\sin\varphi)^2}} \tag{16.21}$$

Obviously, only when Ω equals 0 or π/2 is there no polarisation conversion. This corresponds to one of three special cases; (1) $\varphi = \pi/2$, i.e. the optic axis lying in the incidence plane xoz, (2) $\theta = 0$, i.e. the optic axis being along the x axis, and (3) $\varphi = 0$, $\theta = \pi/2$, i.e. the optic axis being along the y axis. These are exactly the situations mentioned above. Of course the amplitudes and the phases of different order guided modes, propagating in the uniaxial guiding layer are more complex than described above because of the interference between the reflections at the two interfaces. However, whether or not there is creation of polarisation conversion is still essentially correctly described by equation (16.21).

In addition to all the above considerations we may need to incorporate biaxiality, this may be found for the low-symmetry S_C, S_C* and some special nematic phases. In addition in real liquid crystal cells significant variations of the director twist and tilt through the layer will generally exist and these very important situations have to be considered. Thus for most investigation of liquid crystal waveguides simple analytic expressions tend not to be utilised, instead full multilayer optics theory [22-25] is used to model reflectivities, transmissivities and optical field profiles. This then allows the incorporation of the full optical tensor with a spatially varying (through the cell) director profile, allowing the prediction of optical response functions which may be used to compare with data.

Up to now the optical waveguide has only been considered as isolated from the outside environment by infinite dielectric slabs. We now need to describe the experimental procedures used to couple incident radiation into the guiding layer to allow a detailed probing of its optical tensor structure.

16.2.3 Coupling

It is clear that a true guided wave cannot be directly excited by light from the cladding or substrate area unless the light is introduced either from the ends of the guide (end-coupling) or by some secondary mechanism such as fluorescence in the guiding layer. However, end-coupling or fluorescence excitation inside the guiding layer is highly impractical with many

liquid crystal waveguides, thus some light-coupling mechanism, which will inevitably perturb the wavegude, has to be introduced to allow experimental exploration of the waveguide.

For conventional procedures used in laboratories there are, broadly speaking, two mechanisms, prism or grating coupling, for coupling external radiation to the guiding layer. Both give the possibilities of enhancing the momentum of the incident radiation along the propagating direction of the guided waves, essential if the external radiation is to be coupled into a truly guided system. For the first, prism-coupling, the momentum of the incident radiation is enhanced by the refractive index of the prism. The momentum of the incident radiation of the second, grating-coupling, is enhanced by multiples of the grating momentum.

In the prism-coupling procedure a high-index prism is generally used to excite the guided waves by providing the necessary phase matching between the evanescent fields of the incident radiation and a guided wave [26]. A geometry for this type of coupling is shown in Figure 16.6 <Figure 16.6>. A high-index prism, ideally with $n_p > n_g$, is put in close proximity to an air-clad waveguide and radiation is made incident at an incident angle β so that its momentum along the interface matches that of the guided mode, that is

$$k_z = n_p k_0 \sin\beta = \gamma' \tag{16.22}$$

The propagation constant, γ', of the waveguide mode excited via evanescent coupling across the air-gap thickness d is modified from its original value by the proximity of the coupling prism. Of course as the air-gap tends to infinity γ' tends to γ while the coupling tends to zero. In most experiments the incident angle β is varied and the coupling to the waveguide is monitored in some way, then the observed features which correspond to resonant mode coupling can yield information on the mode structure. As shown in Figure 16.6 the true external incidence angle, β', against the entrance face of the prism is related to the internal angle β by the prism angle σ and the refractive index n_p of the prism through

$$\beta' = \sin^{-1}\left[\frac{n_p}{n_0}\sin\left(90^o - \beta - \frac{\sigma}{2}\right)\right] \tag{16.23}$$

where σ is the apex angle of the symmetric prism and $n_0 \approx 1$ is the index of air. According to this equation if incident radiation is normal to the entrance prism face, then for a given β corresponding to the critical angle between the prism and the guiding layer the angle σ satisfies

$$\cos\left(\frac{\sigma}{2}\right) = \frac{n_g}{n_p} \tag{16.24}$$

Thus for a typical guiding layer with an index of the order 1.55 and a prism of index 1.80 a symmetric prism with apex angle of the order 60^o may be used to couple the radiation into the waveguide. This is quite easy to fabricate.

By the same evanescent mechanism which allows the radiation to be coupled into the waveguide the prism can also couple the radiation out of the waveguide. Two independent prisms, one for coupling in and one for coupling out, can be used, particularly if the propagation distance of the guided modes is greater than a few microns and some absorption

aspects of the waveguide are to be investigated. However, for convenience a single symmetric prism is often used for both coupling in and coupling out in standard experiments.

Of course, for practical liquid crystal waveguides, apart from free-standing films, an air coupling gap is not practicable since a constraining wall is needed to contain the liquid crystal. Thus another substance is required to give the low index tunnel barrier, this might be a dielectric, like a silicon dioxide layer, or a thin metallic film, in either case deposited by evaporation on to the base of the prism. For more convenience a similar thin layer may be deposited on to a surface of a high index glass plate which is then index matched with a high index matching fluid to the coupling prism. In this fashion a planar liquid crystal cell can first be fabricated by a normal commercial-like procedure and then studied by optical coupling through a prism and matching fluid. We shall return to the specific geometries needed for liquid crystal studies in the next section.

The second important technique for coupling the incident radiation into the waveguide is grating-coupling [6]. In this arrangement a grating, which may be an amplitude modulation (surface grating) or a phase modulation (index grating), is used to give extra momentum to the incident radiation enabling it to couple to the guided modes. As a simple example to give a basic illustration of the grating coupling effect a grating surface modulated waveguide is shown in Figure 16.7 <Figure 16.7>, in which the grating profile is located at the interface between the waveguide layer and the cladding, although the waveguide-substrate interface will be the same as usual.

If a TE or s-polarised plane wave is incident with an angle β upon such a grating geometry having pitch (or wavelength), Λ and height g as shown in Figure 16.7, then the incident optical field on the interface of the grating may be written

$$E_y = A\{i[(k_0 n_c \sin\beta)z - (k_0 n_c \cos\beta)x - \varpi t]\} \tag{16.25}$$

where A is an amplitude coefficient and, for a sinusoidal grating, we have

$$x = \frac{g}{2}\left(\frac{2\pi z}{\Lambda}\right) \tag{16.26}$$

It is clear that if the boundary between the cladding and guiding layer is a flat surface with x not a function of z, i.e. g = 0, the propagation constant in the z direction will simply be $k_0 n_c \sin\theta$ which will not be big enough, according to the definition of the critical angle for true waveguiding, to couple to guided modes. However if g is finite then at the grating boundary x is a function of z and for a sinusoidal shape of the grating then

$$E_y = A \exp\{ i[(k_0 n_c \sin\theta)z - (\frac{g}{2} k_0 n_c \cos\theta \sin\frac{2\pi z}{\Lambda}) - \varpi t]\} \tag{16.27}$$

and it is obvious that the propagation constant can no longer be readily extracted since there is no simple term just multiplying z in the equation. However, if we expand the above equation in terms of Bessel functions as follows

$$E_y = A \sum_{m=-\infty}^{\infty} J_m(-\frac{g}{2} k_0 n_c \cos\theta) \exp\{ i[(k_0 n_c \sin\theta + m\frac{2\pi}{\Lambda})z - \varpi t]\} \tag{16.28}$$

then the problem can be overcome and, as expected, an infinite series of propagation constants has been introduced in the grating coupling

$$k_{zm} = k_0 n_c \sin\theta + m\frac{2\pi}{\Lambda} \tag{16.29}$$

where m=0, ±1, ±2, etc., gives the order of diffraction.

For the situation of a surface modified by varying gradient the simple planar boundary condition found in Fresnel equations become more complicated. The consequence is that a single incident plane wave will perhaps produce several diffracted plane waves, as well as local evanescent diffracted fields. The coupling mechanism of the grating-coupling is that if we can find an integer m such that k_{zm} is equal to the propagation constant of a waveguide mode then the mode matching condition will be satisfied and some incident radiation may be coupled into this guided mode. Of course the radiation propagating in the waveguide can also equally be coupled out of the guide, just as in the case of evanescent prism coupling. As mentioned above for a planar structure the strength of coupling is dictated by the coupling gap and easy modelled by Fresnel equations. However, for grating-coupling it is the amplitude of the grating which dictates the coupling strength and with a non-planar boundary involved the optics is much more difficult to model and to compare with experimentally recorded data.

In practice these two coupling methods mentioned above can also be combined to give prism-grating coupling systems, or, in addition, holographic couplers [27].

For completeness two other simple coupling methods should also be briefly introduced. One is the end-coupling method [28], in which radiation with a field profile similar in form to the field profile of a guided mode is fed into a waveguide through its end-face. The mode propagation direction in the waveguide is normal to the end-face as shown in Figure 16.8<Figure 16.8>. By using a focusing lens the incident radiation coupling is localised at the end of the waveguide. A high quality, defect free end-face, normally produced by polishing or cleaving, of the waveguide is required in this technique. Thus it will be extremely difficult to arrange a geometry to end-couple incident radiation into a liquid crystal waveguide, even though such a procedure may easily be applied to an optical fibre or a semiconductor laser. Another simple coupling technique is tapered coupling [29]. The principle of this coupling method is illustrated in Figure 16.9<Figure 16.9>. As shown in the picture the incident radiation is coupled by total internal reflection with a zigzag picture into a thin waveguide terminated by a taper. Due to the slowly changing propagation constant in the wedge section of the waveguide end the wavefront is not exactly a plane wave. Because fabricating a cell to give appropriately graded faces to the liquid crystal layer is not particularly easy, this method is also mainly used to couple the radiation into a optical fibre or some solid waveguide in integrated optics.

As mentioned above it is very clear that for the optical probing of liquid crystal waveguides prism or grating coupling are by far the most appropriate techniques. Of course prism-coupling is a simple and convenient method for investigating a fabricated liquid crystal cell, however, grating coupling in some senses is also quite convenient since the grating may be fabricated within the cell during construction and thus no extra optical elements are needed in the study of the cell. In addition aligning liquid crystals in the cell may be achieved by grating and there can be found several studies of the using of grating/liquid crystal geometries [30-33]. However, the cost and the complex procedure of grating fabrication, the extra complexity of the overall optical response of the cell when used as a device may be drawbacks of the grating-coupling technique. In addition the geometry of a liquid crystal waveguide with a grating structure is much more difficult to model

optically by comparison to the rather simple prism-coupled planar geometry. Since only a limited amount of quantitative work has yet to materialise using grating-coupling to detail the director profile in a liquid crystal cell we will largely confine our attention to the prism-coupling technique in the next section.

16.3 Liquid Crystal Waveguide Geometries

From the optical waveguide theory mentioned in the last section the guided mode spectra are sensitive to the parameters of the guiding layer including the profiles of the optical indices (tensor) through the layer and the thickness of the layer. This arises particularly from the fact that each different order mode will be sensitive to different parts of the guiding layer through different optical field distributions for each the guided mode. Of course, this sensitivity is only in one dimension, through the thickness of the guiding layer, but since a mono-domain of liquid crystal in a cell should be invariant in the plane of the guiding layer, then this is exactly the sensitivity required for studying liquid crystal thin films. In addition, comparing with other optical methods the guided mode is the only technique which is going to yield the required spatial selectivity through the thickness of the guiding layer. Over recent years four somewhat different guided mode geometries have been exploited by using prism-coupling to liquid crystal films [34].

For all of the four geometries which are described in more detail below, the essential experimental procedure comprises that of monitoring the angle dependent reflectivity and/or transmissivity of a plane parallel, monochromic linearly polarised optical beam, incident through a coupling-in prism at the glass/liquid crystal layer boundary. According to the optical waveguide models mentioned above, at certain angles of incidence the momentum of the incident radiation along the surface will match that of one of the guiding modes in the layered planar waveguide structure. Then if the geometry is appropriate there will be a reduction in the polarisation-conserving reflectivity at these angles. Of course some related change in the polarisation-conserving transmissivity at these angles will also occur, if another coupling-out prism is used at the bottom of the waveguide structure. Hence by simply monitoring the reflectivity and/or transmissivity as a function of angle of incidence we will find all the mode momentum, the momentum spectra, of the waveguide. These momentum spectra are generally enough to determine the optical properties of the guiding layer for isotropic and lossless materials as may be used in normal integrated optics. However, for a waveguide structure incorporating liquid crystals the situation is more complex. The momentum spectra are only a minimum set of information and although useful, will not readily give the full director profile of the liquid crystal through the cell. If the director is twisted out of the plane of incidence or tilted from the surface the modes in the cell are neither pure TE or TM and the reflected and transmitted radiation will generally have a polarisation converted component. This will not only create polarisation-conversion reflectivity and transmissivity signals but it will also lead to more complex polarisation-conserving reflectivity and transmissivity spectra. More generally, instead of just discussing the mode momentum, one monitors accurately the angle dependent reflectivity (and/or transmissivity) over a wide range of angles and then fits these data to predictions from a multilayer optical model of the geometry. In particular, using angle dependent polarisation conversion reflectivity and/or transmissivity, the sensitivity to the director twist/tilt is greatly enhanced and fitting of this sort of data may yield, in exquisite detail, the director profile through the cell. The resolution of the director profile detail depends on the particular geometry studied, of which, as mentioned above, there are essentially four.

16.3.1 Fully-Guided Geometry

A series of fully-guided modes may be excited in the waveguide having a low refractive index cladding, a high index guiding layer and low index substrate. Although in principal any low index materials can be used as cladding and/or substrate, in general metal-clad waveguides have been the focus of attention in this geometry. There are two main reasons for using metal-clad liquid crystal waveguides in the fully-guided geometry. One is that the metal layers may be used as the electrodes as well as providing a low refractive index ($n_{real} < 1$) and the other is that surface plasmons may be excited at the interface between the metal and the alignment film/liquid crystals. With their exponentially decaying optical fields these surface plasmon excitations can be used to explore the director profile near the aligning surface of the liquid crystals. A typical sample geometry for a metal-clad liquid crystal waveguide is illustrated in Figure 16.10 <Figure 16.10>. This is a nearly symmetric metal-clad dielectric waveguide. In this geometry the thin, about 30-50 nm, metal layer coated directly on to a high index pyramid, acts as both a mirror for trapping guided modes and as a tunnel barrier for radiation coupling. The thickness of this top metal coating is critical and depends on the kind of metal and the wavelength of the radiation. Too thick a metal layer will result in weak coupling to the guided modes, while too thin a layer will allow the guided modes to become more 'leaky' and thus be much broader in angle response, giving a less sensitive experiment. Generally, the metal layer on the substrate is thick enough, optically opaque, to act as a high quality mirror, if the transmission data are not needed. Of course, two aligning films, e.g. SiO_X, are coated on to these metal surfaces respectively to align the liquid crystal in the cell. For suitable coupling of the incident radiation into the guided modes supported by the liquid crystal layer the refractive index of the pyramid should be chosen to have a higher value than any other layer in the geometry. Both high index glass and some high index anisotropic crystal materials, e.g. sapphire, may be used as coupling prisms, although care has to be taken in production to ensure the optic axis of any anisotropic crystal is orthogonal to the plane of incidence.

In this metal-clad waveguide geometry, provided the thickness of liquid crystal layer is greater than the cut-off thickness [6], which is nearly always the case for visible radiation, a series of sharp fully-guided modes should be excited. In addition, with silver (or aluminium, or gold) films acting as mirror surface in the visible, a broader surface plasmon-polariton (SPP) resonance may also be excited [35] at the metal/alignment layer/liquid crystal interfaces using TM polarised incident radiation. While each guided mode is sensitive to different parts of the director profile through the cell, the TM polarised surface plasmon resonance will be sensitive to the director at the aligning surface as well as the optical properties of the aligning film [36]. Further, by switching the input polarisation from TM to TE, the mode spectra become dictated by the transverse optical index of the system and so allow further details of the director profile to be extracted. Hence it is very clear that only using this relatively simple reflectivity-monitoring technique the director profile inside a cell may be unravelled in some detail.

A significant amount of work has been done using this novel technique. For the simple nematic phase, the fully guided technique has been first used to explore the director reorientation at the surface [37] allowing an estimation of the surface anchoring energy [38]. The voltage response of a 90^o twisted nematic (TN) cell has also been explored by the metal-clad waveguide technique [39], while, by the use of pulsed voltages very small field-induced changes in the optical permittivity of a nematic have also been investigated in some detail [40,41]. This has allowed the study of macroscopic director effects as well as other induced order-parameter effects. Other examples include the study of bulk director reorganisation in a nematic having finite surface tilt [42], and a very sensitive measurement of the electro-optic pretransitional effects in the isotropic phase using a differential variant [43] of the direct waveguide technique.

Comparing with studying the rather simple nematic phase the guided mode technique is an even more powerful and important tool for experimentally unravelling the director profile of the more complex chiral smectic C (S_C*) liquid crystal inside cells. By observing the guided mode spectra with the metal-clad fully guided geometry the director alignment in the 'chevron' structure of a surface stabilised ferroelectric liquid crystal (SSFLC) cell was first optically confirmed [44]. For a structure as shown in Figure 16.10 with silver (metal) films, silicon oxide aligning layers and homogeneously aligned layer of ferroelectric liquid crystal (FLC) SCE3 the angle dependent reflectivities have been first experimentally recorded. At a radiation wavelength of 632.8 nm (He-Ne) with a temperature of 31.1°C in the S_C* phase the p-polarised reflectivity (R_{pp}) data as a function of angle of incidence are shown fitted by multilayer optics modelling theory in Figure 16.11[44] <Figure 16.11>. A series of sharp resonance dips in the reflectivity are due to the excitation of fully guided modes in the guiding ferroelectric liquid crystal layer, while the broad resonant dip at about 66° is due to the SPP on the silver/SiO_X/FLC interface. In the case of the alignment direction at the surfaces being parallel to the plane of incidence, Figure 16.11a, some apparent 'mode-splitting' occurs in the guided mode area of the reflectivity curve. This splitting, in the R_{pp} signal, indicates that there is some p to s (or s to p) polarisation conversion, which in turn implies that there is twist of the director out of the original nematic alignment direction as shown in equation (16.21). For the orthogonal plane of incidence, Figure 16.11b, some sharp guided modes appear in the region of the broader SPP resonance dip. This indicates that the twist of the primary director of the FLC is not too far from the surface alignment direction since these s-like guided modes here (from the p to s conversion) have quite large momenta which are close to that of the SPP which is largely dictated by the SiO_X and the situation of the director near the surface. By using multi-layer optics, with the liquid crystal divided into a large number of sub-layers, to carefully fit such angle dependent data in detail, the director profile in the SSFLC cell is found to be largely a uniformly twisted slab, with a twist angle of 13° (from the original nematic alignment direction) with rather limited tilts of less than 2°. Two thin regions of order 100 nm are near both surfaces over which the director twists out from the original alignment direction. This distribution of the optical director across the cell is in good accord with the chevron model of the layers in such a cell found by X-ray scattering [4]. It should be pointed that the smectic layers cannot be directly determined by the optical studies, such as the guided mode technique here, the layer information can only deduced from the director profile determined if the information about the cone angle of the FLC material is also available.

Many fundamental research studies about SSFLC cells have been performed with the metal-clad fully guided geometry, including studies of various SSFLC cells under applied ac and dc electric fields [45-47], half-splayed states [48], including a determination of the low level of optical biaxiality [49]. Further studies have also explored the homeotropically aligned state [50] finding for the smectic A phase that the smectic layers are not necessarily parallel to the cell walls. In view of the high definition of the optical reflectivity response, that is the resonant modes are relatively narrow in angle, the experiments mentioned above have been used to quantify in some detail the director distribution through liquid crystal cells. Thus the metal-clad liquid crystal waveguide technique is a powerful tool for studying the behaviour of liquid crystal inside cells, specially for the more complex ferroelectric phases. Unfortunately there are several limitations that inhibit the usefulness of the metal-clad fully-guided technique for practical device investigation.

Firstly, there are no metal layers in most real devices, and certainly no top, thin, metal film. Secondly, with the relatively soft silver layers it is quite difficult to use the strongly rubbed polymer alignment layers, which are found in most commercial cells on the transparent conducting electrodes (indium tin oxide - ITO) coatings. Even for those situations where quite strong gold films have been used with polymer alignment the alignment created may be different to that with ITO coatings. Thirdly, the thin metal tunnel layer gives very different optical response for the two orthogonal polarisation

directions of the incident radiation, TE and TM. A thin metal layer, such as 40-50 nm of silver as typically used in the visible part of the radiation spectrum, tends to reflect strongly TE radiation. This results in rather weak coupling to TE-like modes in the guiding layer and more especially gives a weak polarisation conversion signals. Since it is just these conversion signals that are particularly sensitive to the director twist and/or tilt, then its weakness limits the detailed determination of the director profile through the cells by this guided technique. A way needs to be found to explore more realistic device-like structures.

16.3.2 Fully Leaky Geometry

It is obvious that if the metallic layers are removed from the previous geometry than all three limitations will be avoided. However this will inevitably mean losing the surface plasmon resonance, and also all of the guided modes will now become leaky. Now the sample geometry becomes that of a liquid crystal layer sandwiched between a pyramid and a glass substrate plate, both with a higher index than the primary index of the liquid crystal and both coated with transparent ITO as a conducting film on top of which are thin transparent rubbed polymer aligning layers as shown in Figure 16.12 <Figure 16.12>. The use of high index pyramid means that there are still critical edges available to help in quantifying the refractive index tensor of the liquid crystal.

For this fully-leaky geometry, when the incident angle β is smaller than the angle for total reflection between the pyramid and the liquid crystal layer, the incident light beam enters the liquid crystal layer and, at the substrate surface, it is partly reflected back into the liquid crystal again with some of the radiation being refracted into the substrate. It is clear that true guided modes cannot be excited and supported in this geometry. However when the electromagnetic wave reflected at the two liquid crystal/glass interfaces satisfies a constructive interference condition then a partial localisation of the radiation inside the liquid crystal layer will occur. Of course, these are fully-leaky guided modes, with propagating radiation leaking out both into the substrate (transmission) and cladding area (reflection). Thus, if the angle dependent reflectivity is once again recorded, then the sharp features obtained from the metal-clad waveguide are now completely absent and a series of much broader resonance will be obtained. However, in a similar fashion to the true guided modes, the electromagnetic waves interfering within the multi-layer system, giving these poorly defined resonances, will also have their own different field distribution across the liquid crystal layer. Hence a study of these fully-leaky modes should also provide details of the director profile through the cell. This type of study is an extension of conoscopy, measuring much higher internal angles of incidence by using a matching fluid and coupling pyramid and also providing much more quantitative information concerning the director profile in a given cell.

This fully-leaky geometry has also been used to explore the director alignment in SSFLC cells [51,52]. A typical set of reflectivity data, compared with a multi-layer optics model is shown in Figure 16.13 <Figure 16.13>. It is as mentioned above, the sharp reflectivity features recorded for the metal-clad fully guided geometry are completely absent and the sensitivity of data fitting to the specifics of the director profile is much reduced. This limits the precision with which the technique may be used to determine the director twist/tilt structure through the cell. However unlike the metal-clad waveguides there is little constraint on the strength of the p to s conversion signal which may then be used to give some further information on the twist/tilt profile of the optical tensor in the cell [53].

Because the fully-leaky geometry uses a simple prism and a matching fluid to couple in radiation it may be applied to commercial-like cells. In addition it also gives good p to s conversion signals for helping to determine the details of director profile through a cell. Thus this fully-leaky geometry should be a favoured technique, if, that is, the serious profile

degeneracy problem arising from fitting model data to the wide modes obtained experimentally can be overcame. However before moving on to an improved fully-leaky guided mode geometry we will first introduce another very powerful technique – the half-leaky guided mode geometry in the next sub-section.

16.3.3 Half-Leaky Guided Mode Geometry

A third variant of the prism-coupled liquid crystal waveguide geometry is the half-leaky guided mode geometry which avoids drawbacks from both of the above geometries and approximates quite well to a real cell geometry, while at same time giving sharper resonant features and strong polarisation conversion signals.

The chosen geometry for the half-leaky guided mode (HLGM) technique is that of a high index glass prism (which may for convenience of cell fabrication be replaced by a prism, matching fluid and a glass plate), ITO coating, rubbed polymer alignment layer, an aligned liquid crystal layer and a low index glass substrate with first ITO coating and then alignment layer on it. It is the asymmetry of the glass index which provides the essential new function of this geometry, since now there are a range of angles of incidence in the upper prism for which light is totally reflected at the liquid crystal/low index glass substrate interface. Thus this interface acts as a perfect mirror (dielectric/dielectric interface beyond critical angle) over a certain angle range providing a half-guided or half-leaky guide system. For this new geometry the high index glass should have an index, n_c, which is greater than the highest index available in the liquid crystal while the low index glass should have an index, n_s, lower than the lowest index available in the liquid crystal. The new half-leaky guided mode geometry is shown in Figure 16.14 <Figure 16.14>. For the convenience of discussion we suppose that the liquid crystal is positive uniaxial with the extraordinary refractive index, n_e, greater than the ordinary index, n_o. This means that the ideal condition of the new geometry is $n_c > n_e$ and $n_s < n_o$. According to the guided mode theory it is obvious that there can be no true guided waves in the liquid crystal guiding layer with these conditions satisfied. However analytical treatment, as well as numerical modelling, of this situation shows [54] that there is a special wavevector range in which there are strong polarisation conversion signals in the reflectivity spectrum. This in-plane wavevector range is between $k_0 n_s$ to $k_0 n'$ where n' is the maximum effective index of the liquid crystal probed by the radiation, $n_o < n' < n_e$. When the angle of incidence (in-plane momentum) is in this window the optical field will be evanescent in the substrate area since $n_c k_0 \sin\beta$ is greater than $n_s k_0$ (so it is beyond the prism/substrate critical angle) while it propagates in the liquid crystal layer because $n_c k_0 \sin\beta$ is less than $k_0 n'$ (so it is below the prism/liquid crystal pseudo-critical angle). In this incident angle window the radiation reflected from the prism/liquid crystal boundary will interfere with that mirror-reflected from the liquid crystal/substrate boundary producing sharp interference features, 'resonances', in the angle dependent reflectivity response. From the illustration mentioned above it is clear that this special wavevector window may be quite narrow between $\beta_s = \sin^{-1}(n_s / n_c)$ and

$\beta' = \sin^{-1}(n' / n_c)$, where $\beta_e \geq \beta' \geq \beta_o$ with $\beta_o = \sin^{-1}(n_o / n_c)$ and $\beta_e = \sin^{-1}(n_e / n_c)$. Then by scanning the incident radiation over this narrow angle window the sharp half-leaky guided mode reflectivity spectra will be experimentally recorded.

Comparing with the fully guided and fully-leaky geometries the major advantages of this half-leaky guided mode geometry are obvious. Firstly, since the high index glass plate has been replaced by a low index one from the fully-leaky geometry then over the limited angle range the optical energy leaking into the substrate is zero. Thus the modes recorded in this range are quite sharp, and are hence more sensitive to the details of the director profile than the fully leaky geometry. Secondly, and possibly more importantly, because there are no metallic coatings needed the test cell can be

constructed following the commercial cell fabrication process with ITO and rubbed polyimide alignment. Thirdly and also associated with the absence of metallic coatings, the polarisation conversion signal may now be quite strong, no longer limited by the reflectivity of the metal layer for TE radiation. This is very important for determining the director profile through cells in detail. If there is director twist and/or tilt from the plane of incidence, then in the half-leaky window strong resonant maxima will be recorded in the angle dependent TM to TE conversion reflectivity. Fitting these data provides even more detail on the twist/tilt director profile across the cell.

The advantages of the HLGM technique have been analysed in detail [54]. From numerical modelling it has been found that the technique has very good sensitivity to all changes in the director twist and tilt, even less than 1^o. It may be used to monitor optical biaxiality as low as 0.0002, and it also gives details of the director configuration quite near the bounding surfaces of the cell.

From the experimental point of view a practical point worthy of note is that although the geometry has to have a high index prism there is no essential need to use very high index glass since for normal liquid crystals the refractive indices are not very high in the visible. We may use an index of 1.73 (632.8 nm, He-Ne) for which matching fluids are available, thus the prism used in the geometry such as shown in Figure 16.14 may then be replaced by a high index upper glass plate, n=1.730, matching fluid (e.g. CH_2I_2) layer, and a high index, n=1.730, prism. The advantage of this arrangement is not only for simpler cell fabrication but it also allows rotation of the cell under the prism thereby guaranteeing, provided there is not simple homeotropic liquid crystal alignment, that some strong TE to TM conversion signal may be obtained by a suitable choice of rotation of the cell. So by using two glass plates with the requisite high and low indices having similar thermal expansion coefficients, so that heating the cell does not cause mechanical stress problems, and following commercial procedures a HLGM test cell can be fabricated and the detailed characterisation of the director profile in such a structure undertaken.

Since the HLGM technique was developed in 1993 [55] a significant amount of work has been undertaken using this powerful tool. The first study, using this technique, was to explore the detailed optical tensor configuration in a homogeneously aligned SSFLC (Merck-BDH SCE3) [55]. In the test cell the aligning surface layers were silicon oxide deposited by evaporation at 60^o to create in-plane homogeneous alignment in the nematic phase. The experimental recorded data has shown as high as 60% p to s conversion reflectivity signals in the incident angle window as discussed above. Using the prediction from Fresnel multilayer optics theory to fit the angular dependent p to s conversion reflectivities yields, in unprecedented detail, the optical tensor configuration through the cell. From the fitting results the director profile of the SSFLC across the cell is that of a slightly bent ‘chevron’ director structure with a small tilt angle of order 1.5^o, with near-surface region of order 0.3 μm in thickness. Additionally a permittivity biaxiality of the FLC material as small as 0.0035 can be found from the fits. In addition information on a small amount of optic tensor axes dispersion is also provided by using two wavelengths, 632.8 nm (He-Ne) and 514.5 nm (Ar-ion) in these experiments.

For this SSFLC cell some typical experimental data for both wavelengths together with theoretical fits are shown in Figure 16.15a and 16.16a, the corresponding director tilt and twist profiles being given in Figure16.15b and 16.16b, respectively <Figure 16.15, Figure 16.16>. From Figure 16.15b and 16.16b it is clear that there are finite tilt surface angles in the cell, which is contrary perhaps to earlier expectations, since Cognard [56] indicates that for 60^o obliquely evaporated SiO_X and a nematic liquid crystal, there will be little surface tilt. It looks like the evidence for tilt with the S_C* phase is overwhelming. From Figure 16.15b and 16.16b the optic tensor axes dispersion with the wavelength of the radiation is also very clear, since there are different tilt angle distributions through the cell for two different wavelengths. The sensitivity of the half-leaky guided mode to the director profile in the cell can be confirmed by a particular example. Consider only the

right hand side of Figure 16.16a, which has been expanded and shown in Figure 16.17a <Figure 16.17>. In Figure 16.17a a particular peak, indicated by an arrow, is very sensitive to director tilt. In this figure three model curves are compared, using the same parameters as used to generate Figure 16.16a except for changes in tilt profile. For the short dashed line the tilt angle is everywhere modelled as zero, for the solid line it is the chosen fit and for the long dashed line it is described in Figure 16.17b by having a maximum tilt of 2^o. It is very clear that the amplitude of this chosen half-leaky guided mode is very sensitive, with resolution much less than 0.5^o, to the director tilt profile across the cell. This also strongly supports the director tensor axes dispersion shown in Figure 16.15b and 16.16b. Comparing with a metal-clad waveguide, in which even though the modes may have been sharper, because of the weakness of the p to s conversion signal by the metal layer, the sensitivity to director twist/tilt profile would be much reduced, the relative value of the HLGM technique is very clear.

The advantage of the sensitivity to the director twist means that the HLGM technique is well suited to the study of the electroclinic effect. This effect has been investigated for a homogeneously aligned S_A phase near to the S_A-S_C* phase transition point. Both materials with first order (material C7) [57] and second order (material C8) [58] transitions have been studied. The extra director tilts induced by the electroclinic effect have been comparing with mean field theory and the electroclinic coefficients have also been quantified. From the experimental results strong surface anchoring constraints are also observed.

Some studies of homeotropic S_C* alignments have also been explored by the HLGM technique. By using a dc in-plane field to unwind the helix of a S_C* homeotropically aligned layer, with or without lecithin surface layers [59-61] the director profile in such cell has been studied. Although the arrangement of the S_C* director should be particularly simple in this geometry the optical results show that, somewhat surprisingly, the smectic layers are not parallel to the cell walls but tilted by as much as 4^o. When the cell is rotated so that the director lies in a plane perpendicular to the plane of incidence a finite p to s conversion signal appears to indicate this layer tilt and this phenomenon can be extended from the S_C* phase up into the S_A phase.

When we use an in-plane dc field to unwind the helical director structure of a homeotropically aligned FLC, then by fitting the reflectivity data recorded the cone angle of the FLC can be accurately obtained for a set of temperatures in the S_C* phase. The extended mean-field theory for a S_C* to S_A transition has been confirmed by the above experimental results [60] and, in addition, detailed information on the optical tensor components of both the S_C* and S_A phases has also been given [62]. In such experiments a p to s polarisation conversion signal can still be recorded even in the S_A phase. This indicates that with respect to the cell wall the layer tilt of the S_C* phase will be retained into the S_A phase [59,61] which would be expected to be aligned with its layers flat in the plane. For a homeotropically aligned FLC with no surface treatment the extra tilt induced in the S_A phase by an in-plane field can be very accurately measured by the p to s conversion signal. Thus it is possible to quantify the electroclinic effect in this almost unconstrained environment, a simple linear relationship between the induced tilt and the dc field being found even under very weak fields [61]. The predictions from a second order Landau mean-field theory, which includes the coupling between the tilt angle and the dc field, has been confirmed in these experiments [61].

From the knowledge of the optical tensor and cone angles obtained for the S_C* material in the homeotropic geometry as mentioned above it will be relatively straightforward to fit with multiplayer optics modelling theory the more complex reflectivity data obtained as the unwinding dc field is removed. This then will give the pitch of the helical S_C* phase at zero voltage applied, and the ratio of the spontaneous polarisation P_S to the twist elastic constant B_3 will be given by fitting the distorted helix for finite fields. In additional P_S can be found from dielectric measurement and then B_3 is readily obtained [63].

The homeotropically aligned smectic C cell has also been studied by the HLGM method [64]. Under the application of an AC voltage the director configuration changes over a time-scale of the order of seconds. Fitting model results to the recorded angle dependent reflectivity data indicates firstly a change of tilt angle of the primary director, suggesting perhaps a layer tilt, and secondly a reduction of the imaginary part of the optical permittivity, implying a suppression of fluctuations. However the expected Helfrich-like deformation is not recorded, with detailed analysis showing not an increase of layer tilt with field but a field-induced increase of cone angle.

The examples given above are mainly for S_C or S_C* phases, since we wished to show the power of the technique for exploring the director structures of complex phases. However, even for some simpler phases, such as the nematic or smectic-A phases, if the director structure is quite complex due to external constraints then the HLGM technique may provide a vital method for determining the profile. Two recent examples are given as follows.

The first concerns the observation of coexisting nematic and smectic-A phases in a twisted liquid-crystal cell [65]. While the properties of twisted nematic cells, which are the important elements of the most widespread electro-optic liquid crystal display devices, are well understood, there is no information about the structure of such cells below the nematic-smectic transition temperature. Since the smectic layers cannot sustain twist the question is what does the system do on cooling? Does it become full of defects or can some other defect-free configuration exist? This phase transformation is also interesting from the fundamental point of view because it represents a nontrivial example of a transition in an inhomogeneous soft system in a confined geometry. The properties of such a transition are expected to be strongly dependent on the cell thickness. So a powerful technique for exploring this is required to accurately determine the director configuration through a thin cell in some detail. As mentioned above the HLGM geometry provides the required technique.

The sample comprises a twisted homogeneously planar-aligned cell with an angle of 87^o between the two rubbing directions of the top and bottom polyimide coated substrates. The liquid crystal material in this study is the ferroelectric liquid crystal SCE13. After filling the liquid crystal in the isotropic phase (~ 110^o C) the temperature is slowly reduced. Upon cooling into the N* phase a well-aligned monodomain forms. Then suitable angle dependent reflectivity, $R_{SS,}$ R_{PP} and R_{SP} (polarisation conversion) data are recorded at different temperatures. From close to the N*-S_A phase transition data are taken at intervals of about 1^o down to the S_C* phase. From fitting the angle dependent reflectivity data recorded several points have been obtained. Firstly, as expected, in the N* phase a uniformly twisted director profile is found in the cell. Secondly, from the data taken on slow cooling it is easy to identify the N* to S_A phase transition point by the sudden appearance, between 67.0 and 67.8^o C, of an extra optical mode feature in the HLGM reflectivity spectrum. Thirdly, when the temperature is lower than the N* to S_A phase transition point there is still a good monodomain in the cell which is conformed by the very good guided mode features in the $R_{SS,}$ R_{PP} and R_{SP} reflectivities and very low background in the R_{SP} data. Finally, in the temperature range of the S_A phase the director profile has a very different form to the linearly twisted nematic. For a thinner cell with thickness of 1.60μm an untwisted homogeneous region forms in the centre of the cell. This has been identified as a region of S_A material. This S_A area is separated from the walls by thin regions of nematic with a higher twist gradient than before the S_A nucleated. Upon further cooling the thickness of the S_A region grows at the expense of the nematic as shown in Figure 16.18 <Figure 16.18>. For increased cell thickness more separated S_A areas appear in the cell. For the 2.0 μm cell there are two regions of uniform azimuthal angle (S_A phase) separated by a twisted nematic with two twisted nematic boundary regions as shown in Figure 16.19(a), while for the 2.4 μm cell there are three S_A regions separated by two twisted layers with two twisted boundary layers as shown in Figure 16.19(b) <Figure 16.19>. The uniqueness of the director profile through these test cells can only be achieved by the HLGM technique, since it is very sensitive to the variation of the director twist/tilt distributions across the cells. So the director profiles discovered in

this work gives a picture of coexisting nematic and smectic-A phases in a twisted liquid crystal cell. The experimental results also show that comparing with the bulk phase sequence of the FLC material the S_A phase exists over a very small temperature range in these twisted thin cells. This suppression in phase transition is caused by the high twist gradient in the liquid crystal and has to be expected since the S_A phase cannot tolerate any twist. A theoretical model of these novel results is also presented in the work [65] to give a complete explanation.

The second example concerns establishing the direction of the 'easy' axis at a twisted nematic liquid crystal wall determined by the half-leaky guided mode technique [66]. For the measurement of surface torsional or azimuthal anchoring energy, which is very important both from the fundamental science perspective as well as for the production of display devices, a geometrical technique using a thin twisted nematic (TN) cell has been widely used. Since no external field is needed to distort the director profile in the cell both the mathematics and the experimental procedures are quite simple. In this TN geometry the twist-off of the director at the surface of the cell is brought about by equilibrium between the two surface torsional anchorings mediated through the bulk twist elastic constant, K_{22}. From continuum theory the key numbers required to quantify the torsional anchoring strength are the elastic constant K_{22}, the gradient of the twist angle, $d\phi/dz$, and the deviation of the twist angle from the easy axis, $\phi-\phi_e$, at the wall of the TN cell. K_{22} is measured separately (given in the chemical suppliers data sheet) and the $d\phi/dz$ can be obtained from the total twist angle of the liquid crystal director, ϕ_t, through the thin TN cell and the LC layer thickness, d_{LC}, by $d\phi/dz = \phi_t/ d_{LC}$. Then half of the difference between the two angles ϕ_t and ϕ_t^0, which is the angle between the two easy axes on the two interfaces of the cell, is taken as the deviation of the twist angle at both boundaries, if the alignments are assumed to be identical. Both ϕ_t and d_{LC} can be accurately determined in the geometrical technique using for example the HLGM technique. However, when a thin TN cell has been assembled the twist angles of the director on the two boundaries always deviate from the easy axes, hence accurate determination of ϕ_t^0 is not simple. It is in fact much easier to measure ϕ_t rather than ϕ_t^0. It is apparent that after rubbing the polyimide, assembling the cell and mounting it on a sample holder an accurate and direct determination of the easy axes directions of a TN cell is very important to allow characterisation of the surface torsional anchoring force by the geometrical technique.

From numerical modelling using continuum theory for a thin TN cell it is apparent that under high voltage (a typical value for a practical cell about 4-5 volts) the gradient $d\phi/dz$ near both surfaces is zero. This is because in the middle part of the cell the director, driven by the high electric field, is almost homeotropically aligned. This removes the influence of the two boundaries from each other through the twist elastic constant K_{22}, i.e. now the direction of the director at the wall will coincide with the direction of the easy axis. Thus all that is required is some optical procedure for determining this director direction at the surface when a suitable voltage has been applied to the cell. There are three factors which may be used to determine the direction of the director at the surface: (1) For an interface between an isotropic and a uniaxial anisotropic medium if the optic axis of the uniaxial medium is in the incidence plane there will be no polarisation conversion reflectivity signal. By contrast a very small angle of optic axis twist out of the incidence plane creates a small but detectable polarisation conversion signal in the reflected beam. (2) If the director of the top surface is close to the incidence plane of the radiation beam then in the HLGM geometry there is a pseudo-critical angle dependent on the high index of the isotropic medium and the low ordinary index of the uniaxial medium. Also in an incident angle range beyond this pseudo-critical angle, for a s-polarised incident beam the optical field in the anisotropic medium exponentially decays away from the interface. (3) For a practical TN cell at high voltages the director lies in the direction of the easy axis for a distance of about 0.5 μm which is much greater then the decay distance mentioned above. Thus there will be no p to s (or s to p) conversion within this depth if the director lies in the incidence plane. According to the above three factors an

experimental procedure is designed to accurately measure the easy axis at the cell surface [66]. Firstly matching fluid is placed between a high index prism and the top glass plate of the HLGM cell to allow the cell to be freely twisted against the incidence plane with the rubbing direction set near to the incidence plane. Then with the incident angle set greater than the pseudo-critical angle and under a high ac voltage (4.0 volts, 1.0kHz) the p to s polarisation conversion reflectivity signals are recorded for different cell twist angles. The minimum point of the polarisation conversion reflectivity signal accurately gives the director direction, the easy axis direction, at the top surface of the cell. The experimental results of the polarisation conversion reflectivity against the easy axis twist angle from the incidence plane are shown in Figure 16.20[66] <Figure 16.20>. Using this procedure the surface torsional anchoring coefficient between a nematic liquid crystal (E7-BDH) and a rubbed polyimide layer has been determined [67].

All of the above applications of the HLGM technique show quite clearly that it is a very powerful procedure for exploring the optical tensor configuration of a liquid crystal in a thin cell. However, this powerful technique still has a limitation, i.e. the two glass plates from which the test cell is comprised are very different from each other and from commercial cell glass. So if the director profile of a real commercial device cell, which has low index, normally 1.52, glass plates, is to be explored by a guided mode technique, some further improvement is still required.

16.3.4 Improved Fully-Leaky Guided Mode Geometry

If a standard commercial-like liquid crystal cell with low index glass plates is to be investigated by a guided mode technique to unravel the director profile through the cell, then only the low index fully-leaky guided mode (FLGM) technique may be chosen. As mentioned before, because all the guided modes will now be leaky and will give correspondingly broad features in the reflectivity data, this may severely limit the precision with which the director twist/tilt structure through the liquid crystal cell may be determined. In addition, the use of low index glass means that no longer will there be any critical angle available to help determine the refractive indices of the liquid crystal. However, recently some improvements [21] have been introduced to the fully-leaky geometry, in which two refinements to the original technique have been made to make it much more useful. Firstly, the full sets of both transmission, T, and reflection, R, data may be utilised, including all the polarisation-conversion signals R_{SP}, R_{PS}, T_{SP} and T_{PS} as well as the polarisation- conserving signals R_{PP}, R_{SS}, T_{PP} and T_{SS}. The polarisation-conversion signals are particularly sensitive to the director twist and tilt. Secondly, two matching prisms with matching fluid have been used to allow rotation of the cell to a position that allows optimisation of sensitivity to director twist and tilt. In addition, this allows the acquisition of data for a set of different azimuthal angle settings that, by fitting of all the data sets, further removes ambiguity in determining the director profile.

The new FLGM geometry is shown in Figure 16.21 <Figure 16.21>. As mentioned above this is a symmetrical structure in which two identical low index prisms with matching fluid couple the radiation in and out from a symmetrical commercial-like liquid crystal cell comprised of two low index glass plates with suitable ITO coatings and alignment layers on their inner surfaces. Of course, comparing with the other three geometries an extra detector and an extra polarizer are needed in the experimental arrangement for detecting suitable transmission signals.

Since the improved FLGM technique was introduced in 1999 [21] a substantial body of work has been done using this technique to investigate the commercial-like liquid crystal cells. To demonstrate the potential use of this new technique for the determination of the director profile in a liquid-crystal layer, a conventional surface-stabilised ferroelectric liquid crystal cell has been studied [21]. The glass of the cell is ordinary glass with an index close to 1.52, as are the two coupling

prisms. The sample used in this study contains the ferroelectric liquid crystal SCE8*. The alignment is homogeneous with a slight pretilt achieved by the use of rubbed polyimide in a parallel arrangement. The glass plates, which are 1 mm thick and coated with ITO on the inner face, have an index of 1.517 at 632.8 nm. All measurements were conducted on a monodomain at room temperature, 23.7^{o} C. Experimental data, including the polarisation-conserving signals (R_{PP}, R_{SS}, T_{PP} and T_{SS}) and the polarisation-conversion signals (R_{SP}, R_{PS}, T_{SP} and T_{PS}), are recorded with the cell configured so that the surface-alignment axis (rubbing direction) is close to the plane of incidence. An example of the polarisation-conversion reflectivity signals, R_{SP} and R_{PS}, are shown in Figure 16.22 <Figure 16.22>. From Fig. 16.22 we note that these R_{SP} and R_{PS} signals are quite weak, being less than 1%. This indicates that the director of the ferroelectric liquid-crystal layer is only twisted a small amount from the alignment direction. Also note that there are differences between R_{SP} and R_{PS}, which implies a small tilt angle of the director through the cell.

To theoretically model the optics of this cell structure and thereby predict the observed optical response, a scattering-matrix approach has been employed with the liquid-crystal being represented as 150 sub-layers. These sub-layers are part of an overall model structure that treats the liquid crystal as having several (up to 10) boundary matched regions in which the director twist and tilt vary linearly. This linear variation is represented by both start and finish tilt and twist angles and a layer thickness. This procedure reduces the number of variables for the liquid crystal layer to two real and imaginary permittivities and ten sets of linked layer parameters. The final director profiles, obtained by fitting the recorded data with the predictions from the multi-layer optics, are shown in Figure 16.23(a) and (b) <Figure 16.23>, in which there is a clear director-tilt chevron close to the centre of the cell with thin boundary layers with the liquid crystal being in the C2U state [68]. The smectic layer tilt, δ, may also be extracted by using a value for the cone angle of 19.50^{o} at 23.7^{o}C (BDH-Merck data) combined with the profiles of Figure 16.23 (a) and (b)[55]. The resulting layer tilt profile, the layer chevron, is shown in Figure 16.23(c). This shows primarily two tilts that are slightly different in the two parts of the cell. For the lower, slightly thicker, portion the layer tilt is 16.70^{o} and for the thinner upper portion it is 17.30^{o}. There is also a discernable, but small variation of this tilt near the upper bounding surface.

Thus it is clear that the new FLGM technique, using both reflectivity and transmissivity signals, is capable of giving details of the director profile in a commercial-like cell to almost the same level of precision as had been previously obtained by use of either metal-clad guiding structure or cells with different index glass plates in the half-leaky geometry. Unlike the other two procedures, there are no very sharp features in the angle-dependent signals owing to the weak (leaky) nature of the guiding; furthermore, there are no true critical angles to yield the refractive indices of the liquid crystal because the glass of the cell and the coupling prisms have such a low index (1.517). Nevertheless, there is sufficient information in the eight data sets available at each azimuthal angle of study to yield all the requisite information. This means that more detail can still be extracted regarding the spatial distribution of the director profile through the cell by the new FLGM technique.

After this first demonstration of the improved fully-leaky technique some commercially-like standard liquid crystal cells have also been investigated. This includes the quantification of the azimuthal anchoring energy [69] and the surface- and bulk-order parameters [70] of a homogeneously aligned nematic liquid crystal under an in-plane electric field, and the determination of the polar anchoring energies of both homogeneously [71] and a homeotropically [72] aligned nematic liquid crystals. Some mixed alignment liquid crystal cells, which have a zero-order grating alignment on the superstrate and rubbed polyimide alignment on the substrate, have also been studied by this new technique to investigate the influence of the groove depth of the grating on the alignment [73] and the torsional anchoring energy [74]. Because the new technique allows the use of standard liquid crystal cells then combined X-ray scattering and fully-leaky guided mode

studies have been undertaken to explore the smectic layer and the optic tensor configuration in a ferroelectric liquid crystal cell [75]. All of this work, using the guided mode technique to explore conventional commercial-like cells, paves the way for detailed exploration of the behaviour of such cells under various conditions and also allows dynamic studies.

16.4 Dynamic guided mode technique

As mentioned in the above sections the success of the guided mode techniques in determining the director distribution through a thin liquid crystal layer can be attributed to the fact that each optical mode has a different field intensity profile across the liquid crystal layer. Thus a clear 'pictures' of the director across the thin cell can be 'observed' by the results of fitting the recorded angle-dependent reflectivity and/or transmissivity data with the predictions from multi-layer optic theory. From both a fundamental scientific perspective and also for device development the switching process of a liquid crystal layer under an external voltage is very important. Thus establishing a clear picture of the transient director profile through a cell as it varies on time scales of order ms, the dynamic director profile, is very important. It is also obvious that the guided mode technique would be an attractive tool for this dynamic director profile determination. Some early studies successfully resolved the dynamic director profile across the liquid crystal cells in a metal-clad fully-guiding geometry [76,77]. However, like the vast majority of liquid crystal waveguide techniques mentioned before, these studies were based upon the standard angle-scan collimated beam procedure. The experiment is a fairly simple optical arrangement in which a plane polarised collimated laser beam is incident through a coupling prism onto the liquid crystal cell. By rotating the liquid crystal cell and prism arrangement around an axis perpendicular to the incident wave vector, the angular dependent reflectivity and transmissivity features are recorded. Of course, this is a relatively slow data acquisition procedure, every switching process has to be repeat again for every rotating step, i.e. every incident angle, taking anywhere from several minutes to 2 hours to perform a single angle scan [77]. These ponderous studies of dynamic processes using a slow angle scan with time dependent data taken at each angle demand highly repeatable voltage cycling of the cells, complete thermal stability and total lateral invariance within a given cell. Thus an improved guide mode technique has been developed for fast dynamic studies.

The new approach involves the use of a convergent beam and has several advantages over the standard collimated beam angle scan procedure [78,79]. This convergent beam guided mode (CBGM) technique uses a highly focused beam spot that allows simultaneously the excitation of many guided modes and produces reflectivity and transmissivity data over a wide incident angle range. There are several advantages to this procedure. Firstly the CBGM technique removes the need to physically rotate the liquid crystal cell geometry and consequently the focused beam remains completely stationary on the liquid crystal layer. This allows the study of cells with lateral non-uniformity, opening up the potential for single pixel studies.To demonstrate the usefulness of the technique with either half-leaky [80] or fully-leaky [81] geometries the static director profiles for nematic liquid crystal cells have been determined. Secondly, possibly even more importantly, data from the converged beam technique may be captured with a suitable charge coupled device (CCD) array in a time equal to the line transfer rate of the CCD array (< 0.1 ms for a typical array). Thus using a convergent beam technique, data may be acquired around five to six orders of magnitude faster than using the collimated beam procedure, allowing for real time studies of liquid crystal dynamics by the guided mode technique.

Since the fully leaky geometry allows the study of standard commercial-like liquid crystal cells the first COGM study [16] of liquid crystal dynamics was undertaken with the improved fully leaky guided mode geometry. In this study the cell consisted of two ordinary glass plates (n= 1.52) coated with ITO upon which is a rubbed polyimide layer. The rubbing

directions on the top and bottom plates are antiparallel, thus inducing a uniform, nearly planar alignment of the director through the cell. The cell is filled with the nematic liquid crystal ZLI-2293 (Merck). For directly coupling the convergent beam in and out from the sample geometry two low index hemispheres are optically matched onto the cell by use of a suitable low volatility silicon based oil as shown in Figure 16.24 <Figure 16.24>. The use of the matching fluid not only provides a continuous optical medium for coupling light into and out of the waveguide modes but also enables the cell to be easily rotated to any azimuthal angle for optimising sensitivity to director twist and tilt.

The experimental set-up of the COGM technique is shown in Figure 16.25 <Figure 16.25>. The He-Ne laser beam (632.8 nm, 75 mW) is expanded, polarised, and focused through the hemisphere onto the liquid crystal layer. The reflected and transmitted beams are then captured with a linear CCD array (DALSA SPARK). The diffuser arrangement situated in the beam expander serves two purposes. First, it breaks up the spatial and temporal coherence of the laser, and second, it provides an intensity profile across the expanded beam such that approximately the same intensity is available to excite each guided mode. The dynamic study in this work uses an integration time of 0.3ms and therefore it is desirable for the rotating diffuser to complete at least one whole revolution in this time. A turbine dental drill (LARES APOLLO557) was used and once properly adapted gave a diffuser rotation rate of 120,000 rpm (period ~0.5 ms).

Initially, the total of eight data sets of the reflectivity and transmissivity were taken with no voltage and 1.5 V rms (10 kHz) applied to the cell to characterise the static optical parameters of the liquid crystal cell. Once the optical parameters of the LC cell and the static director profile at 0 and 1.5 V had been ascertained by fitting the data recorded with multi-layer optics theory, the dynamics of the director profile as it relaxes from the 1.5 V to the 0 V configuration was studied. The switching dynamics of the LC cell were recorded by synchronising the CCD array to capture data when the voltage across the LC cell was changed. After removal of the voltage both R_{PP} and R_{SS} signals were captured as a function of time and fitted together. The fitted experimental data for the R_{PP} and R_{SS} signals and the corresponding director profiles used to obtain each least squares fit are shown in Figure 16.26 <Figure 16.26>. From the fitting results the tilt of the director in the middle of the cell against time can be extracted and then the exponentially decaying time constant of the relaxation process is revealed to be $\tau = 51.4 \pm 0.1$ ms. Then, from the relation between the time constant, τ, the thickness of the cell, d, the splay elastic constant, K_{11}, and the effective rotational viscosity, γ^*, the γ^* value is deduced. Using a value for K_{11} of 12.75 pN and a d value of 6.63 μm (determined from the static fits), γ^* is evaluated to be 0.147 ± 0.003 Pas at 20.0^o C. By using the same experimental arrangement as mentioned above the 'back-flow' phenomenon of the relaxation process in a twisted nematic liquid crystal cell, which was theoretically predicted by Berreman [82] in 1975 and indirectly confirmed by an optical 'bounce' in the light transmission [83,84], has now been directly and clearly 'observed' from the dynamic director profiles [17].

These experiments clearly show that the COGM arrangement with the FLGM geometry is a very powerful technique for investigating dynamic processes within liquid crystal cells in detail.

16.5 Conclusions

The distribution of the liquid crystal optical permittivity tensor, the director profile, through an aligned cell and its static or dynamic response to changes in environment (applied dc, ac or pulsed electric field, surface anchoring, temperature, cell geometry, etc.) is one of most important aspects of liquid crystal science. Much fundamental understanding, material parameter determination and device design procedures are dependent upon the knowledge of the director profile and its changes under various conditions. Because of the nature of optical guided modes the liquid crystal waveguide techniques

provide an extremely powerful method for studying this tensor profile in detail allowing exploration of both static and dynamic processes.

In this chapter first the principles of optical guided waves in general have been described with some discussion of optical field profiles, coupling procedures, etc., this has been followed by a fuller discussion of several types of waveguiding techniques used to investigate liquid crystals in aligned cells. These techniques include that of the metal-clad fully guiding geometry; the fully-leaky waveguide with no metal layers but which gives poor resolution; the half-leaky waveguide technique which again has no metal layers but which yield sharper optical features giving much finer detail of the director profile; the improved fully-leaky guided mode technique which can be directly used to investigate a commercial-like standard liquid crystal cell and still gives enough information for characterising the director profile through such cells, and finally the convergent beam guided mode technique with the improved fully-leaky geometry to directly and rapidly study the dynamic process in a standard liquid crystal cell. A range of experimental results using these techniques have been presented to illustrate their usefulness with a range of cells structures and liquid crystal phases.

All these guided mode techniques are very powerful tools for exploring the static or, very recently, the dynamic director profiles and determining the optical or physical properties of thin liquid crystal films. Which technique is chosen is dependent on the sample and the information required. However it seems likely that the advantages of being able to use off-the-shelf cells will see progressively more use of the fully-leaky technique. It is very clear that by using a wide range of incident angles and multilayer optics theory to fit the obtained data in these guided mode techniques some of the uncertainties and erroneous conclusions associated with integrated techniques (e.g. simple crossed polariser microscopy), which often ignore the surface layers, are avoided. However, it should be added that, dependent on the sample geometry and the measurements taken, the guided mode technique may require elaborate data analysis based on the Berreman transmission/reflection matrix and a complex fitting procedure to obtain the required results. It is essential that sufficient consideration is given to the sample geometry suitable for obtaining the information required and as many of the unknown parameters are pre-determined by other procedures before any one particular optical guided mode technique is chosen.

In this review chapter we have chosen not to discuss to any length the other very interesting and useful technique, grating-coupling of radiation into guided modes. This is primarily because this needs special cell fabrication and also the theoretical analysis of the optics is much more complicated. By contrast the prism-coupled procedures discussed use simple planar multilayer optics theory, leading to accurate detailed comparisons of predicted responses with those observed experimentally. This leads to substantial confidence in the director profiles thus deduced, which is fundamentally why these guided wave procedures provide an underpinning to liquid crystal science.

Acknowledgement

The authors are extremely grateful to the project 10174044 supported by NSFC.

References

[1]. F Reinitzer, *Monatsh. Chem.,* vol.9 (1888) p.421.

[2]. O Z Lehmann, *Phys. Chem.,* vol.4 (1889) p.462.

[3]. M A Handschy and N A Clark, *Appl. Phys. Lett.,* vol.41(1982) p.39.

[4]. T P Rieker, N A Clark, G S Smith, D S Parmar, E B Sirota and C R Safinya, *Phys. Rev. Lett.,* vol.59(1987) p.2657.

[5]. P K Tien, *Appl.Opt.,* vol. 10 (1971) p.2395.

[6]. D Marcuse (Ed.), *Intergrated Optics,* IEEE Press, New York, (1973).

[7]. H A Weakliem, D J Channin and A Bloom, *Appl. Opt.,* Vol.14 (1975) p.560.

[8]. D J Channin, *Appl. Phys. Lett.,* Vol.22 (1973) p.365.

[9]. J P Sheridan, J M Schnur and T C Giallorenzi, *Appl. Phys. Lett.,* vol.22 (1973) p.561.

[10]. J P Scheridan, *OSA Topical Meeting on Integrated Optics,* New Orleans, (1974) TUA S-1.

[11]. Chenming Hu, J R Winnery and N M Amer, *IEEE J. Quan. Elect.,* vol. QE10 (1974) p.218.

[12]. R B Meyer, *Mol. Cryst. Liq. Cryst.,* vol.40 (1977) p.33.

[13]. N A Clark and S T Lagerwall, *Appl. Phys. Lett.,* vol.36 (1980) p.899.

[14]. L Z Ruan, M A Osipov and J R Sambles, *Phys. Rev. Lett.* vol.86 (2001) p.4548.

[15]. Fuzi Yang and J R Sambles, *Jpn. J. Appl. Phys.,* vol.37 (1998) p.3998.

[16]. N J Smith and J R Sambles, *Appl. Phys. Lett.,* vol.77 (2000) p.2632.

[17]. N J Smith, M J Tillin and J R Sambles, *Phys. Rev. Lett.,* (2002), accepted.

[18]. Fuzi Yang, J R Sambles and G W Bradberry, *The Optics of Thermotropic Liquid Crystals,* Eds. S J Elston and J R Sambles , Taylor & Francis, London, (1998) ch.5.

[19]. M S Kharusi, *J. Opt. Soc. Am.,* vol.64 (1974) p.27.

[20]. Fuzi Yang and J R Sambles, *J. Opt. Soc. Am. B,* vol.11 (1994) p.605.

[21]. Fuzi Yang and J R Sambles, *J. Opt. Soc. Am. B,* vol.16 (1999) p.488.

[22]. R M A Azzam and N M Bashara, *Ellipsometry and Polarised Light*, Amsterdam, North Holland, (1979).

[23]. M Born and E Wolf, *Principle of Optics,* Oxford, Pergamon, (1964).

[24]. J Lekner and M C Dorf, *J. Opt. Soc. Am. A*, vol.4 (1987) p.2092.

[25]. D Y K Ko and J R Sambles, *J. Opt. Soc. Am. A*, vol.5 (1988) p.1863.

[26]. J H Harris, R Shubert and J N Pelky, *J. Opt. Soc. Am.,* vol.60 (1970) p.1007.

[27]. E A Ash, E Seaford, O Soares and K S Pennington, *Appl. Phys. Lett.,* vol.24 (1974) p.207.

[28]. R Shubert and J H Harris, ***IEEE** Trans. Microwave Theory Tech.,* vol.**MTT-16** (1968) p.1048.

[29]. N H Hartshorne and A Stuart, *Crystals and the Polarising Microscope,* 2nd edn., London, Arnold, (1950).

[30]. A Sugimura and T Kawamura, *Jan, J. Appl. Phys.,* vol.23 (1984) p.137.

[31]. Y Kawata, K Takatoh, M Hasegawa and M Sakamoto, *Lig. Cryst.,* vol.16 (1994) p.1027.

[32]. G P Bryan-Brown, J R Sambles and K R Wolford, *J. Appl. Phys*., vol.73 (1993) p.3603.

[33]. E L Wood and J R Sambles, *J. Mod. Opt.,* vol.40 (1993) p.493.

[34]. Fuzi Yang and J R Sambles, *Physical Properties of Liquid Crystals:Nematics,* Eds. D Dunmur, A Fukuda and G Luckhurst (INSPEC-The Institution of Electrical Engineers Publication, London, United Kingdom, 2001) ch.7.3.

[35]. E Kretschmann, *Z. Phys.* vol.241 (1973) p.313.

[36]. G J Sprokel, R Santo and J D Swalen, *Mol. Cryst. Liq. Cryst.,* vol.68 (1981) p.29.

[37]. K R Welford, J R Sambles and M G Clark, *Liq. Cryst.,* vol.2 (1987) p.91.

[38]. K R Welford and J R Sambles, *Appl. Phys. Lett.,* vol.50 (1987) p.871.

[39]. Lizhen Ruan, S J Eolston and J R Sambles, *Liq. Cryst.,* vol.10 (1991) p.369.

[40]. Lizhen Ruan, G W Bradberry and J R Sambles, *Liq. Cryst.,* vol.11 (1992) p.655.

[41]. Lizhen Ruan, G W Bradberry and J R Sambles, *Liq. Cryst.,* vol.12 (1992) p.799.

[42]. Lizhen Ruan, T W Preist, Fuzi Yang and J R Sambles, *Liq. Cryst.,* vol.13 (1993) p.541.

[43]. E L Wood, J R Sambles and P S Cann, *Liq. Cryst.,* vol.16 (1994) p.983.

[44]. S J Elston, J R Sambles and M G Clark, *J. Mod. Opt.,* vol.36 (1989) p.1019.

[45]. S J Elston and J R Sambles, *Appl. Phys. Lett.,* vol.55 (1989) p.1621.

[46]. S J Elston, J R Sambles and M G Clark, *J. Appl. Phys.,* vol.68 (1990) p.1242.

[47]. S Ito, F Kremer, E Aust and W Knoll, *J. Appl. Phys.,* vol.75 (1994) p.1962.

[48]. S J Elston and J R Sambles, *Jpn. J. Appl. Phys.,* vol.29 (1990) L641.

[49]. S J Elston and J R Sambles, *Mol. Cryst. Liq. Cryst.,* vol.220 (1992) p.99.

[50]. M N Gong, J R Sambles and Fuzi Yang, *Liq. Cryst.,* vol.13 (1993) p.637.

[51]. C R Lavers and J R Sambles, *Ferroelectrics,* vol.113 (1991) p.339.

[52]. C R Lavers and J R Sambles, *Jpn. J. Appl. Phys.,* vol.30 (1991) p.729.

[53]. C R Lavers and J R Sambles, *Liq. Cryst.,* vol.8 (1990) p.577.

[54]. Fuzi Yang and J R Sambles, *J. Opt. Soc. Am. B,* vol.10 (1993) p.858.

[55]. Fuzi Yang and J R Sambles, *Liq. Cryst.,Opt.,* vol.13 (1993) p.1.

[56]. J Cognard, *Mol. Cryst. Liq. Cryst.,* vol.78 (1981) Supplement.

[57]. Lizhen Ruan, J R Sambles, E L Wood and J Seaver, *Liq. Cryst.,* vol.18 (1995) p.401.

[58]. Lizhen Ruan, J R Sambles and J Seaver, *Liq. Cryst.,* vol.19 (1995) p.133.

[59]. Fuzi Yang and J R Sambles, *Mol. Cryst. Liq. Cryst.,* vol.250 (1994) p.143.

[60]. Fuzi Yang, G W Bradberry and J R Sambles, *Phys. Rev. E,* vol. 50 (1994) p.2834.

[61]. Fuzi Yang, J R Sambles and G W Bradberry, *Liq. Cryst.,* vol.18 (1995) p.407.

[62]. Fuzi Yang, J R Sambles and G W Bradberry, *J. Appl. Phys.,* vol.78 (1995) p.2187.

[63]. Fuzi Yang, G W Bradberry and J R Sambles, *Phys. Rev. 53,* vol. 53 (1996) p.674

[64]. Lizeen Ruan, J R Sambles and J M Towler, *Liq. Cryst.,* vol.18 (1995) p.81.

[65]. L Z Ruan, M A Osipov and J R Sambles, *Phys. Rev. Lett.,* vol.86 (2001) p.4548.

[66]. F Z Yang, H F Cheng, H J Gao and J R Sambles, *J. Appl. Phys.,* vol.88 (2000) p.4553.

[67]. F Z Yang, H F Cheng, H J Gao and J R Sambles, *J. Opt. Soc. Am. B,* vol.18 (2001) p.994.

[68]. N Itoh, M Koden, S Miyoshi and T Wada, *Liq. Cryst.,* vol.15 (1993) p.669.

[69]. B T Hallam, Fuzi Yang and J R Sambles, *Liq. Cryst.,* vol.26 (1999) p.657.

[70]. B T Hallam, C V Brown and J R Sambles, *J. Appl. Phys.,* vol.86 (1999) p.6682.

[71]. Fuzi Yang, J R Sambles, Youmei Dong and Hongjin Gao, *J. Appl. Phys.,* vol.87 (2000) p.2726.

[72]. Fuzi Yang, Lizhen Ruan and J R Sambles, *J. Appl. Phys.,* vol.88 (2000) p.6175.

[73]. B T Hallam and J R Sambles, *Phys. Rev. E,* vol. 61 (2000) p.6699.

[74]. B T Hallam and J R Sambles, *Liq. Cryst.,* vol.27 (2000) p.1207.

[75]. B Hodder, J R Sambles, S Jenkins and R M Richardson, *Phys. Rev. Lett.,* vol.85 (2000) p.3181.

[76]. M Mitsuishi, S Ito and M Yamamoto, *J. Appl. Phys.,* vol.81 (1997) p.1135.

[77]. M Mitsuishi, S Ito and M Yamamoto, *Appl. Phys. Lett.,* vol.69 (1996) p.2199.

[78]. E Kretschmann, *Opt. Commun.,* vol.26 (1978) p.41.

[79]. J R Sambles and N J Smith, *Mol. Cryst. Liq. Cryst.,* vol.347 (2000) p.37.

[80]. N J Smith and J R Sambles, *J. Appl. Phys.,* vol.85 (1999) p.3984.

[81]. N J Smith and J R Sambles, *Mol. Cryst. Liq. Cryst.,* vol.347 (2000) p.45.

[82]. D W Berreman, *J. Appl. Phys.,* vol.46 (1975) p.3746.

[83]. C J Gerritsma, C Z van Doorn and P van Zanten, *Phys. Lett. A,* vol.48 (1974) p.263.

[84]. F Nakano, H Kawakami, H Morishita and M Sato, *Jap. J. Appl. Phys.,* vol.19 (1980) p.659.

Figure captions

Fig. 16.1 The geometry of a planar optical waveguide, with cladding area, guiding layer and substrate area.

Fig. 16.2 Guided optical modes in a planar waveguide: (a) full guided mode, (b) substrate radiation mode, and (c)substrate-cladding radiation mode.

Fig. 16.3 The optical electric field profile, perpendicular to the mode propagation direction, for different TE modes propagating in a planar waveguide with different propagation constants. (a) substrate-cladding radiation mode, $\gamma < k_0 n_c$, (b) substrate radiation mode, $k_0 n_c < \gamma < k_0 n_s$, (c) guided mode with $k_0 n_s < \gamma < k_0 n_g$.

Fig. 16.4 The field distributions for TE modes, produced by equations (16.11) and (16.12), with mode orders of m=0, m=1 and m=2. The corresponding ray optics models are also shown in each case.

Fig. 16.5 Geometry for an isotropic-uniaxial anisotropic-isotropic system.

Fig. 16.6 Geometry for a prism-coupled waveguide system, with a low index tunnel barrier of thickness w.

Fig. 16.7 Geometry of a grating-coupled waveguide structure. The grating wavevector $2\pi/\Lambda$ adds momentum to the incident radiation allowing it to couple to the guided mode.

Fig. 16.8 Geometry of an end-coupled system for a waveguide in which a lens is used to focus the incident beam of radiation onto the end of the guiding layer.

Fig. 16.9 The tapered-coupling geometry for waveguides where the light is converted by reflection from being radiative to being totally internally reflected in the guiding layer.

Fig. 16.10 The geometry for a metal-clad liquid crystal waveguide. Here a thin metal film on the high index pyramid acts as a tunnel barrier and the metal film on the substrate is optically thick.

Fig. 16.11 The reflectivity for p-polarised light from a homogeneously aligned ferroelectric liquid crystal, SCE3, cell, in the S_C* phase at 31.1° C , with the surface alignment direction (a) parallel and (b) perpendicular to the plane of incidence. The solid lines indicate the fit of the data (crosses) to theory. The cell walls, first coated with silver, are overcoated with silicon oxide (evaporated obliquely at 60°) to form an aligning layer. The cell was 3.5 μm thick and measurements were made at λ = 632.8 nm. (From [44]).

Fig. 16.12 Geometry for a fully leaky liquid crystal waveguide. The pyramid and substrate both have refractive indices greater than the liquid crystal layer.

Fig. 16.13 Typical reflectivity results for a ferroelectric liquid crystal in the S_C* phase at 38.3° C, using p-polarised radiation at λ = 632.8 nm. The solid line shows the fit of data (crosses) to theory. In this case rubbed polyimide was used to provide the alignment layers. (From [51]).

Fig. 16.14 Geometry for the half-leaky guided mode (HLGM) method with a high index prism and low index substrate.

Fig. 16.15 (a) The p to s conversion reflectivity from liquid crystal SCE3 using the HLGM technique with a wavelength of 632.8 nm. The solid line indicates the fit of theory to the experimental data (shown as crosses). (b) The twist and tilt profile in the cell determined from fitting the experimental data . (From [55]).

Fig. 16.16 (a) The experimental p to s conversion reflectivity obtained at 514.5 nm using the same cell as for Figure 16.15. (b) Twist and tilt profiles determined by fitting experimental data to theory. (From [55]).

Fig. 16.17 (a) Angular dependent reflectivity, for a wavelength of 514.5 nm, obtained by theoretical modelling using the twist profile in Figure 16.16(b) and the tilt angle profiles shown in Figure 16.17(b). (b) The tilt angle profiles used to generate the theoretical curves shown in Figure 16.17(a). The reflectivities and

corresponding profiles are indicated by the different dashed lines. (From [55]).

Fig. 16.18 Director twist angle profiles $\phi(z)$ across the 1.6 μm twisted liquid-crystal cell obtained using the half-leaky guided-mode method for three different temperatures. (1) T = 67.0°C; (2) T = 66.3°C; (3) T = 65.8°C. Note the untwisted region in the centre of the cell which is identified as a region of smectic-A material that grows with decreasing temperature. The insert shows a schematic of the geometry of the experiment. (From [65]).

Fig. 16.19 Director twist angle profiles $\phi(z)$ in the 2.0 μm twisted cell with two separate smectic-A regions (a), and in the 2.4 μm cell with three smectic-A regions (b). (From [65]).

Fig. 16.20 Experimentally recorded reflectivity data R_{PS} from 62.5° to 65.0° of incident angle for a TN cell at 4.0 volts. (a) Six R_{PS} curves which correspond to the director in the incident plane and twisted away by 1.0°, 2.0°, 4.0°, 5.0° and 6.0° from bottom to top, respectively. (b) Six R_{PS} curves which correspond to the director in the incident plane and twisted by same angles in the opposite direction as (a). (c) The intensity of a selected p to s conversion mode against the twist-off angle of the director from the incident plane of the radiation. (From [66]).

Fig. 16.21 The two prism-coupling cell geometry of the improved fully-leaky guided mode technique.

Fig. 16.22 Experimentally recorded reflectivity conversion data, R_{PS} and R_{SP}, (crosses) and fitted theory curves (solid line) for a SCE8* cell. (From [21]).

Fig. 16.23 Fitted profile of the director in the SCE8* layer : (a) Twist angle measured from the incident plane, (b) Tilt angle measured from the plane parallel to the cell wall, and (c) Layer tilt angle calculated with a cone angle of 19.50° together with the twist/tilt profiles. (From [21]).

Fig. 16.24 The geometry for hemispherical coupling to a conventional FLGM cell.

Fig. 16.25 The experimental set-up of the convergent beam guided mode technique.

Fig. 16.26 Left column and middle column: fits to the transient R_{SS} and R_{PP} signals, respectively, for various times. Right column: the corresponding director profile used to obtain fits to experimental data. (From [16]).

Ch.16 Guided mode ... Fuzi Yang and J R Sambles

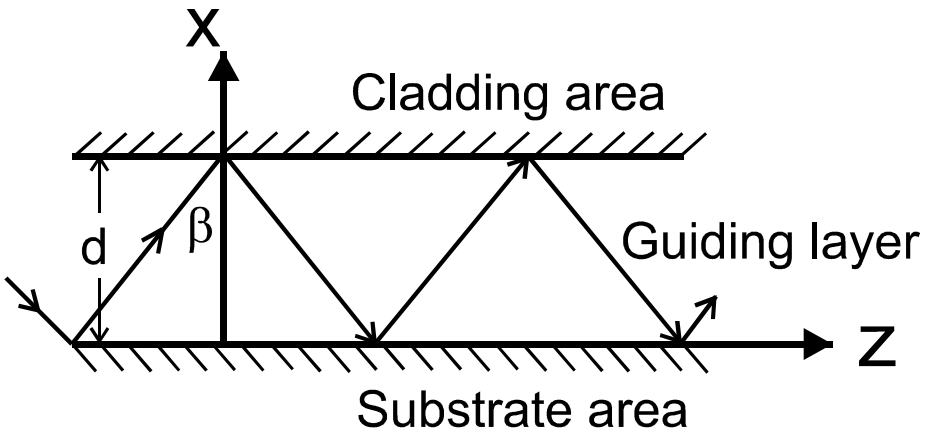

Fig. 16.1

Ch.16 Guided mode ... Fuzi Yang and J R Sambles

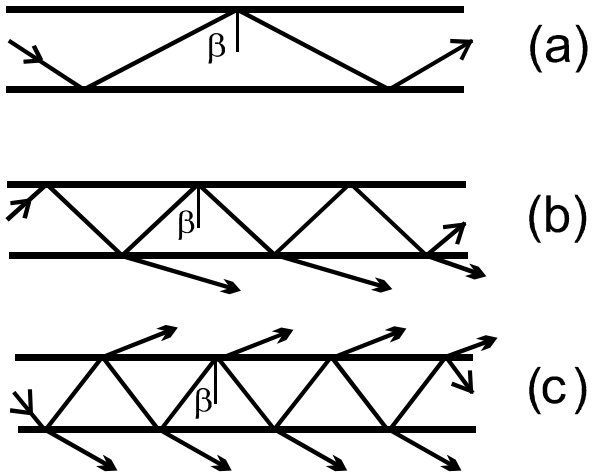

Fig. 16.2

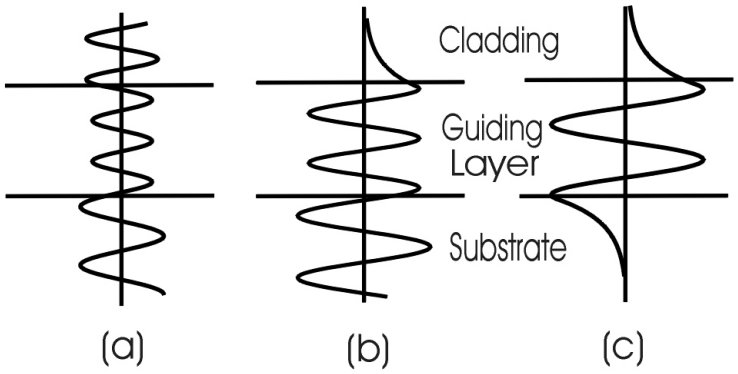

Fig. 16.3

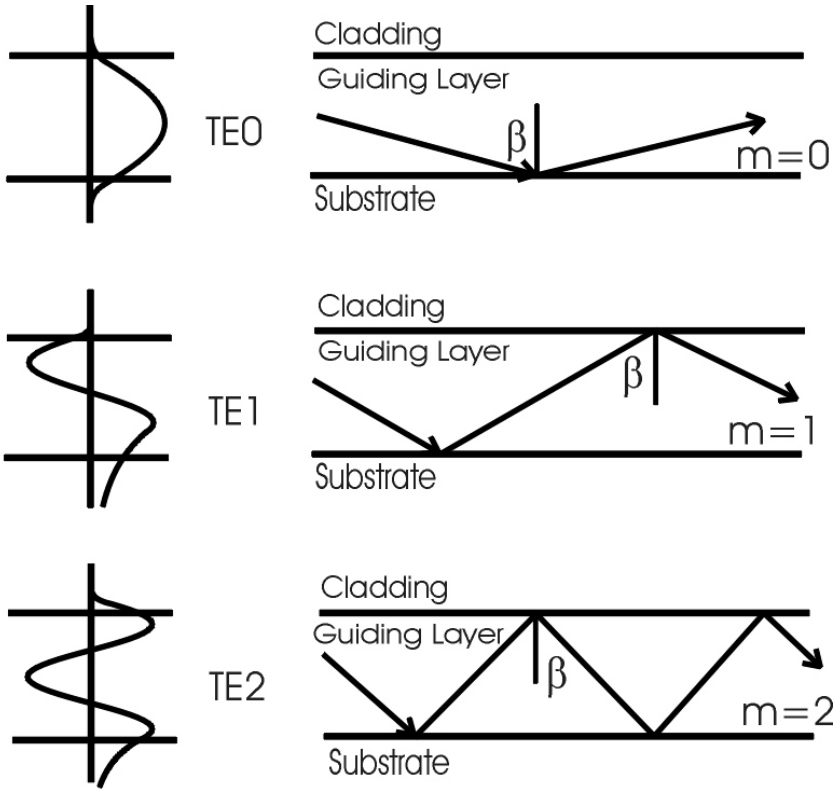
TE0
Cladding
Guiding Layer
β
m=0
Substrate
TE1
Cladding
Guiding Layer
β
m=1
Substrate
TE2
Cladding
Guiding Layer
β
m=2
Substrate

Fig. 16.4

Ch.16 Guided mode ... Fuzi Yang and J R Sambles

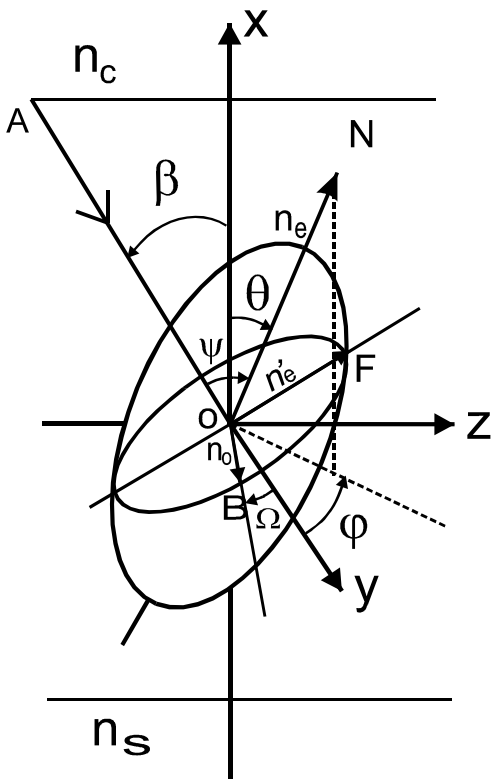

Fig. 16.5

Ch.16 Guided mode ... Fuzi Yang and J R Sambles

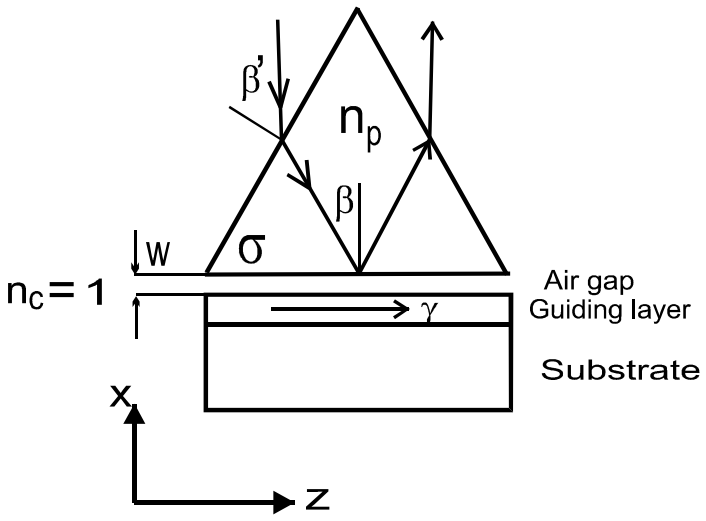

Fig. 16.6

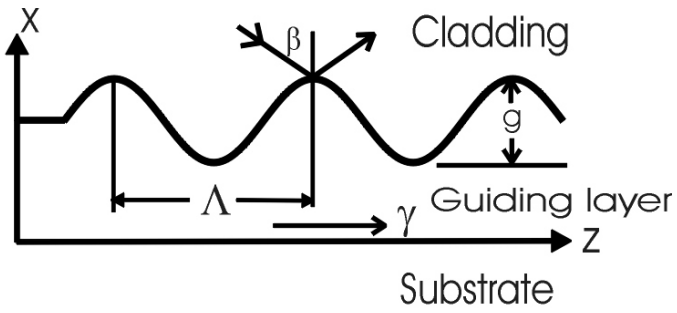

Fig. 16.7

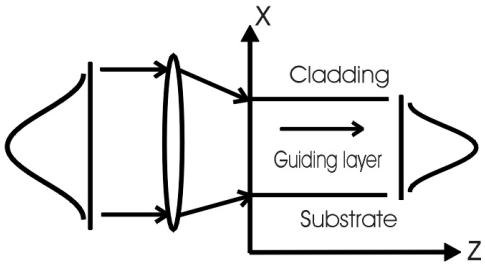

Fig. 16.8

Ch.16 Guided mode ... Fuzi Yang and J R Sambles

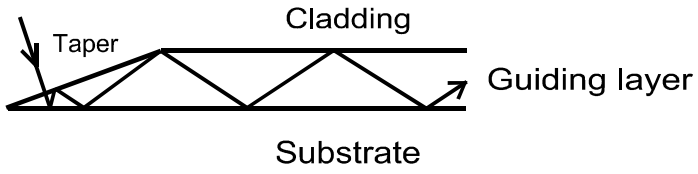

Fig. 16.9

Ch.16 Guided mode ... Fuzi Yang and J R Sambles

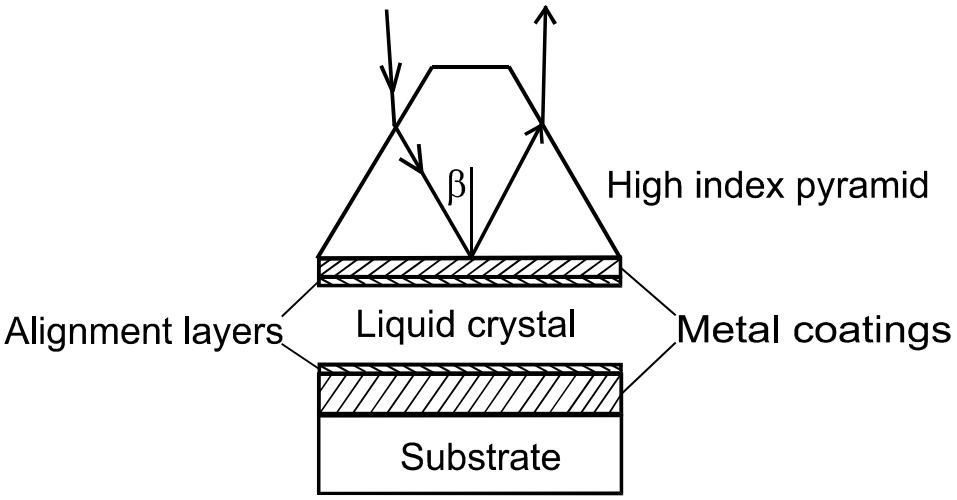

Fig 16.10

Ch.16 Guided mode ... Fuzi Yang and J R Sambles

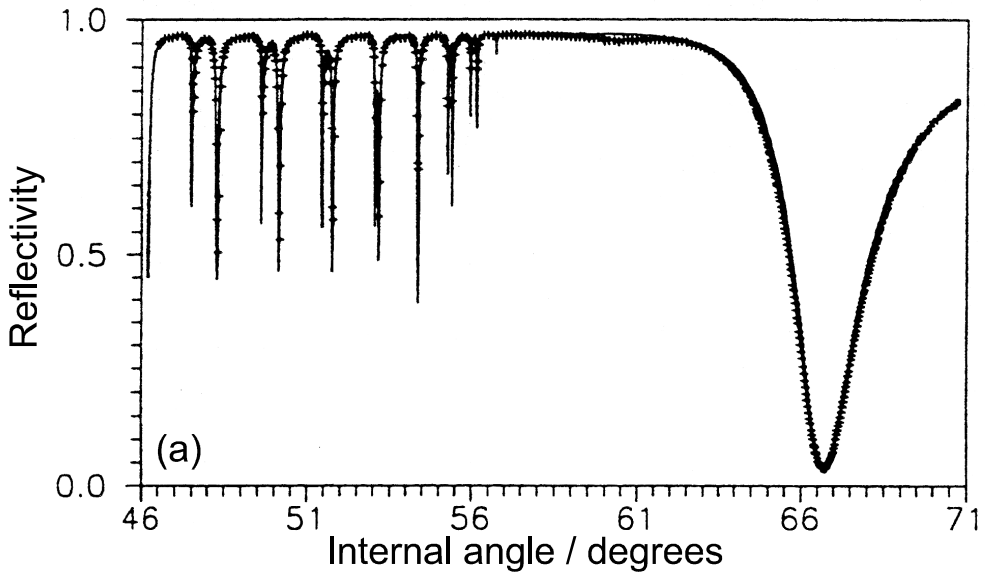

Fig. 16.11(a)

Ch.16 Guided mode ... Fuzi Yang and J R Sambles

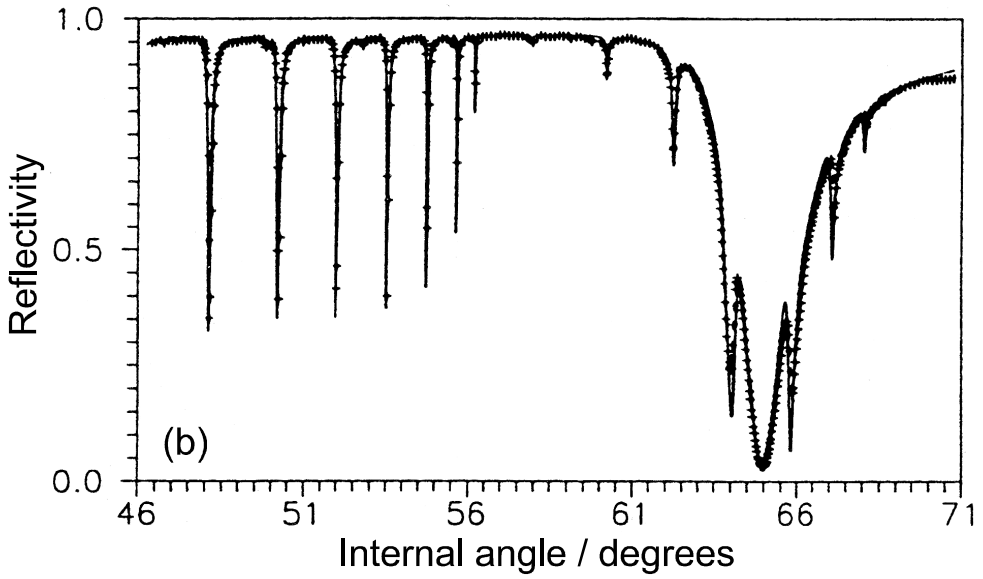

Fig. 16.11(b)

Ch.16 Guided mode ... Fuzi Yang and J R Sambles

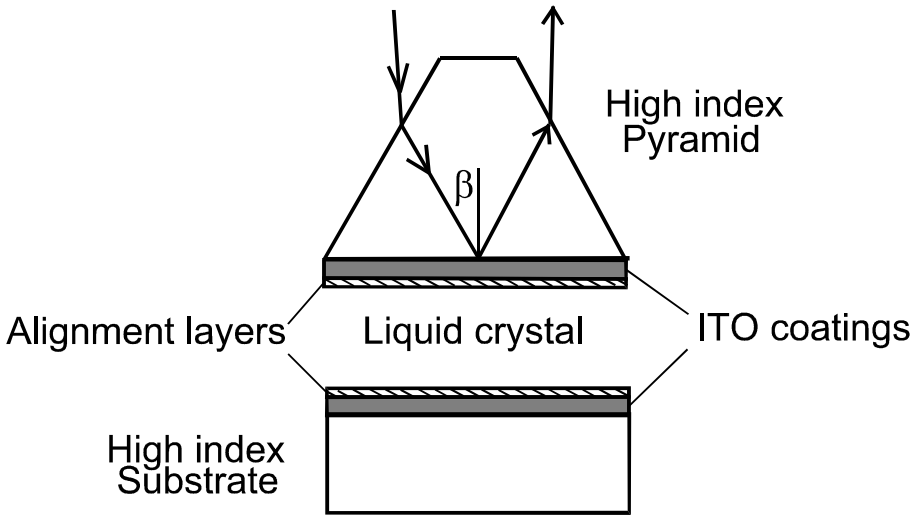

Fig. 16.12

Ch.16 Guided mode ... Fuzi Yang and J R Sambles

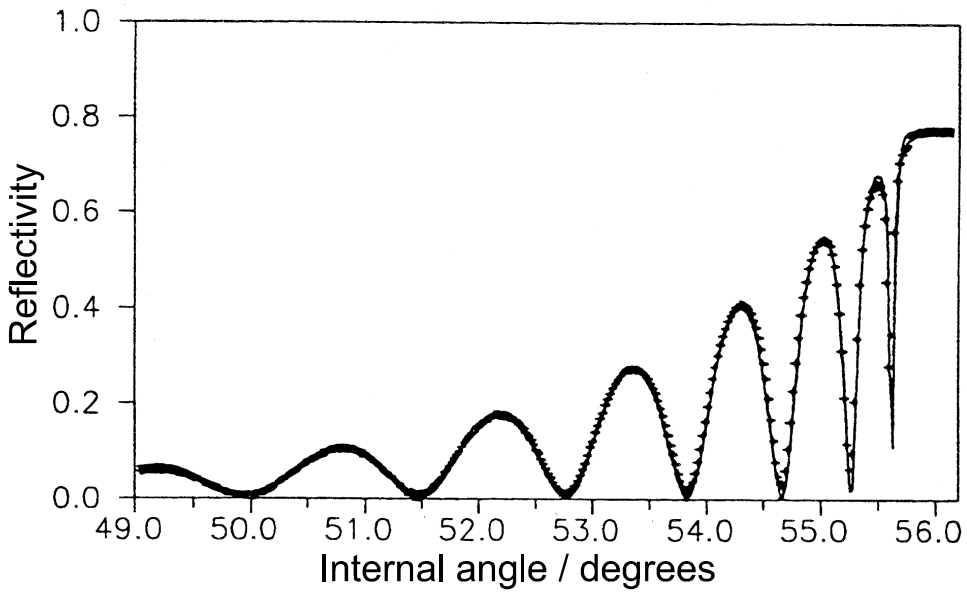

Fig. 16.13

Ch.16 Guided mode ... Fuzi Yang and J R Sambles

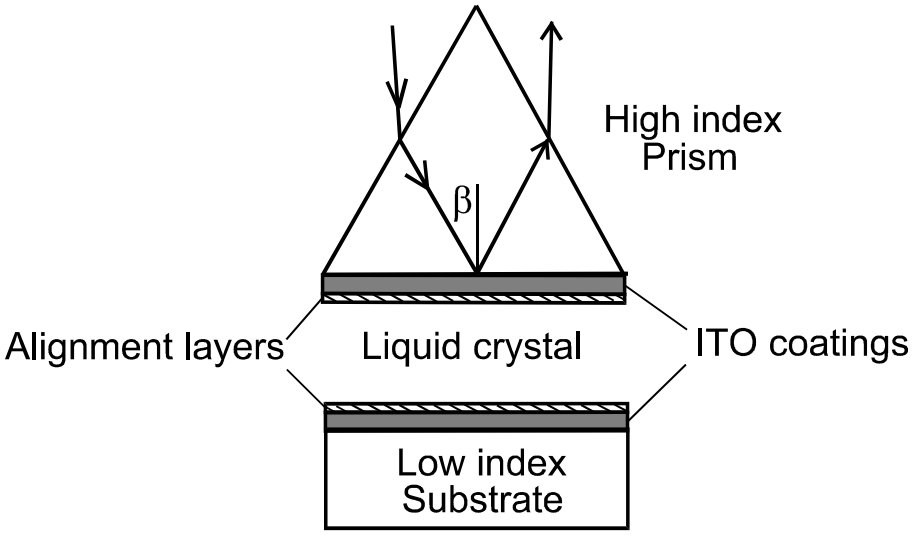

Fig. 16.14

Ch.16 Guided mode ... Fuzi Yang and J R Sambles

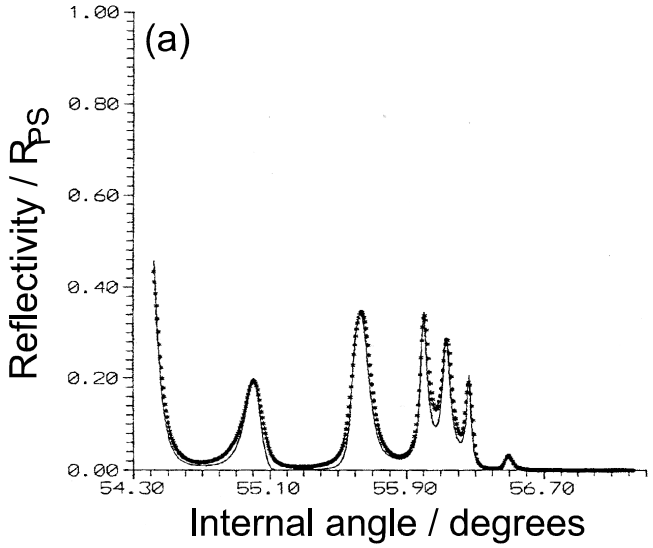

Fig. 16.15(a)

Ch.16 Guided mode ... Fuzi Yang and J R Sambles

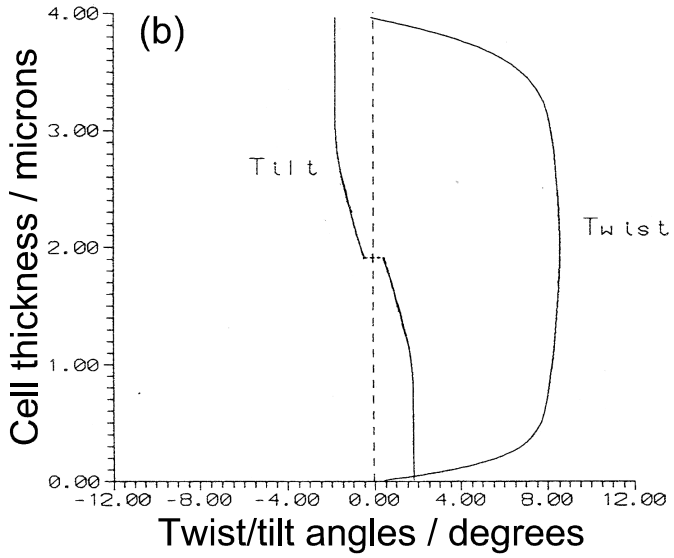

Fig. 16.15(b)

Ch.16 Guided mode ... Fuzi Yang and J R Sambles

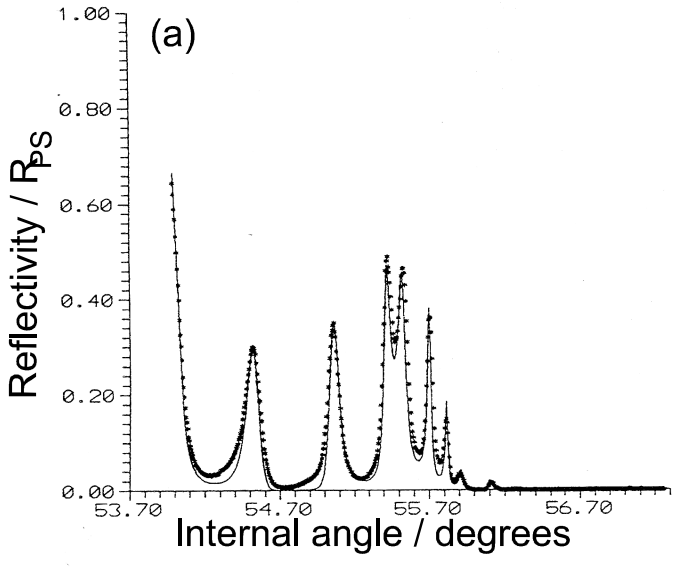

Fig. 16.16(a)

Ch.16 Guided mode ... Fuzi Yang and J R Sambles

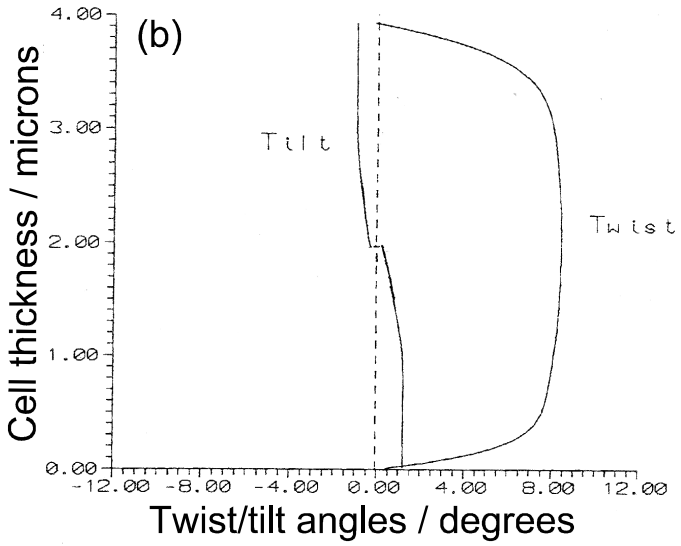

Fig. 16.16(b)

Ch.16 Guided mode ... Fuzi Yang and J R Sambles

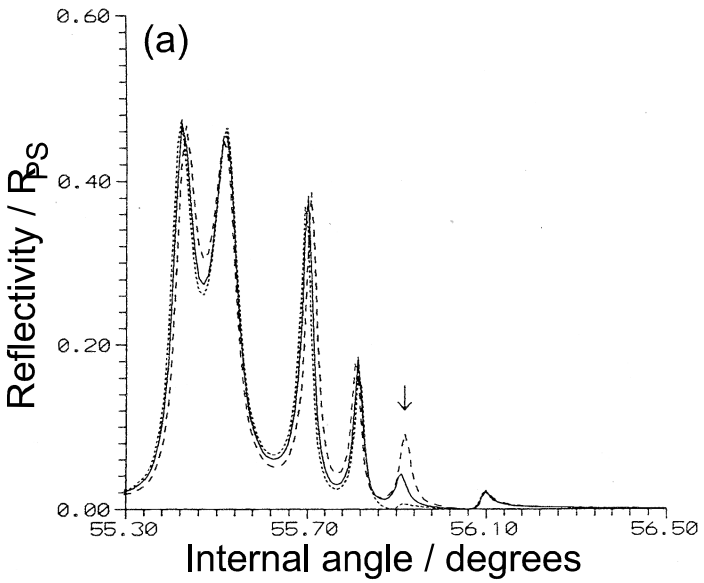

Fig. 16.17(a)

Ch.16 Guided mode ... Fuzi Yang and J R Sambles

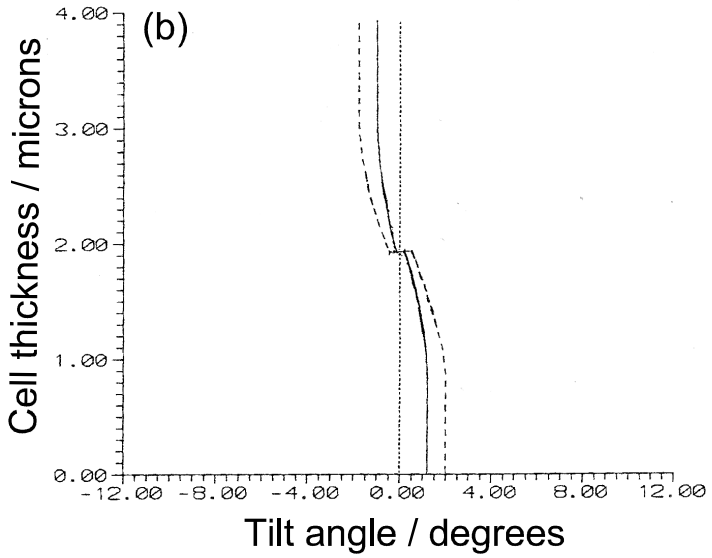

Fig. 16.17(b)

Ch.16 Guided mode ... Fuzi Yang and J R Sambles

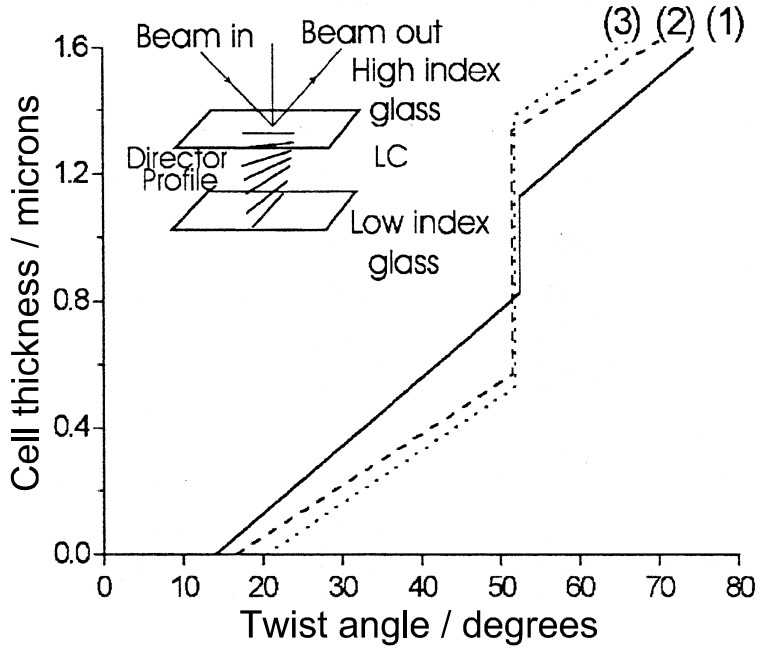

Fig. 16.18

Ch.16 Guided mode ... Fuzi Yang and J R Sambles

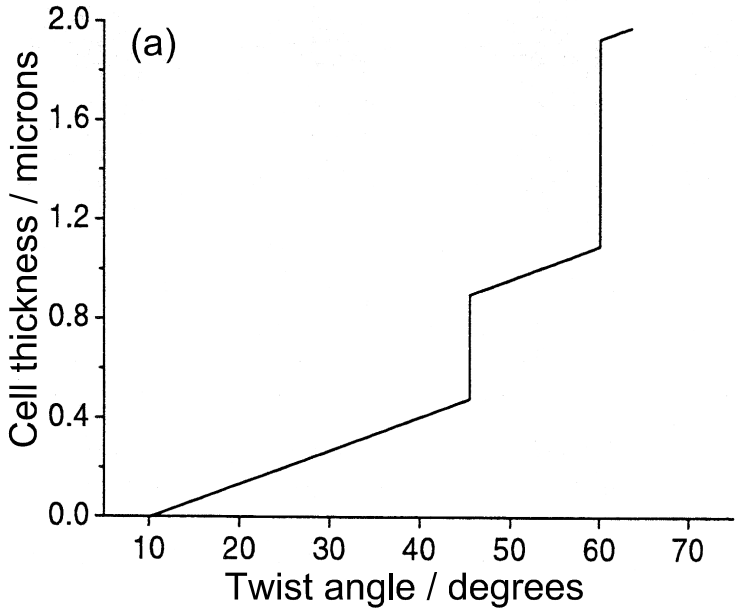

Fig. 16.19(a)

Ch.16 Guided mode ... Fuzi Yang and J R Sambles

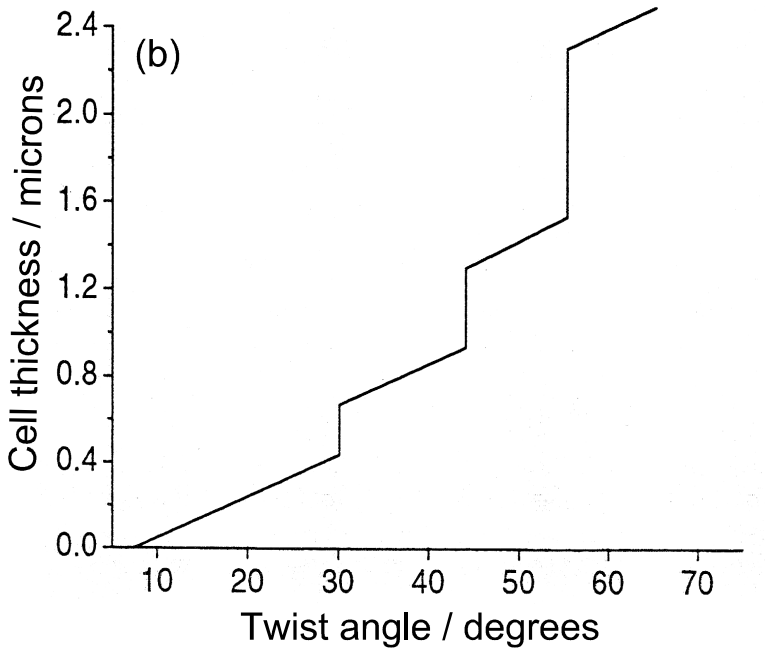

Fig. 16.19(b)

Ch.16 Guided mode ... Fuzi Yang and J R Sambles

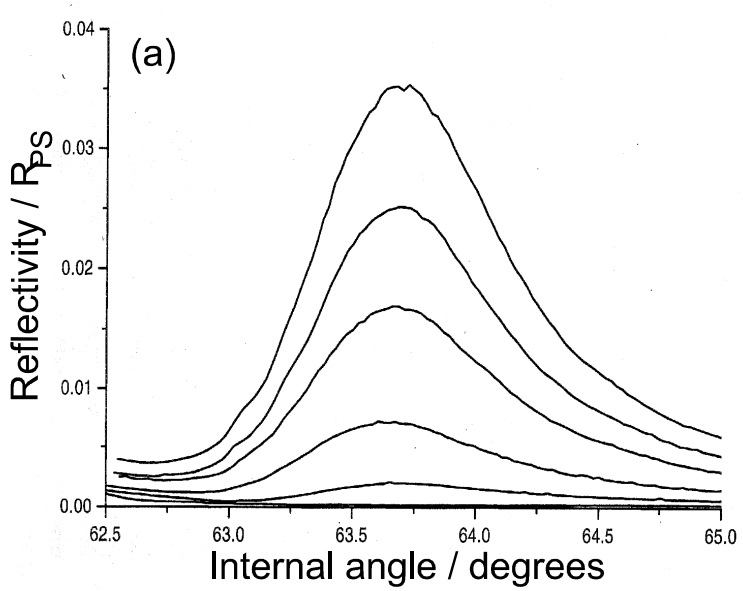

Fig. 16.20(a)

Ch.16 Guided mode ... Fuzi Yang and J R Sambles

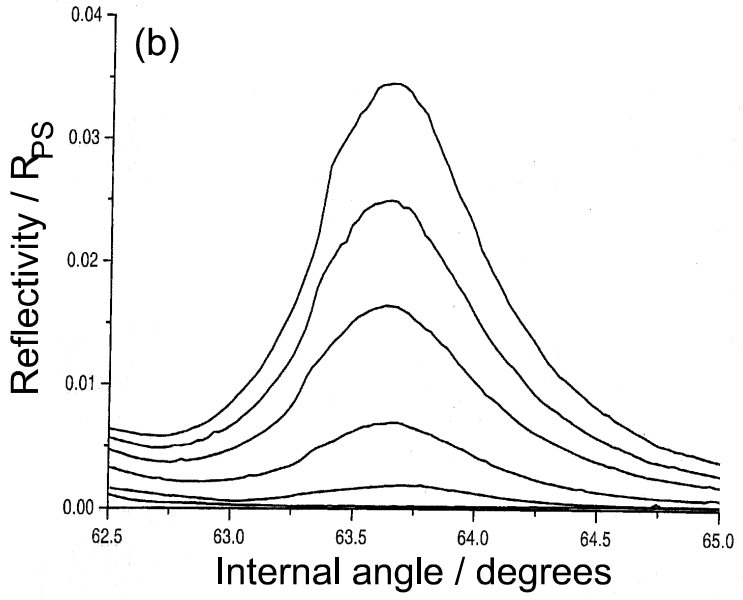

Fig. 16.20(b)

Ch.16 Guided mode Fuzi Yang and j r sambles

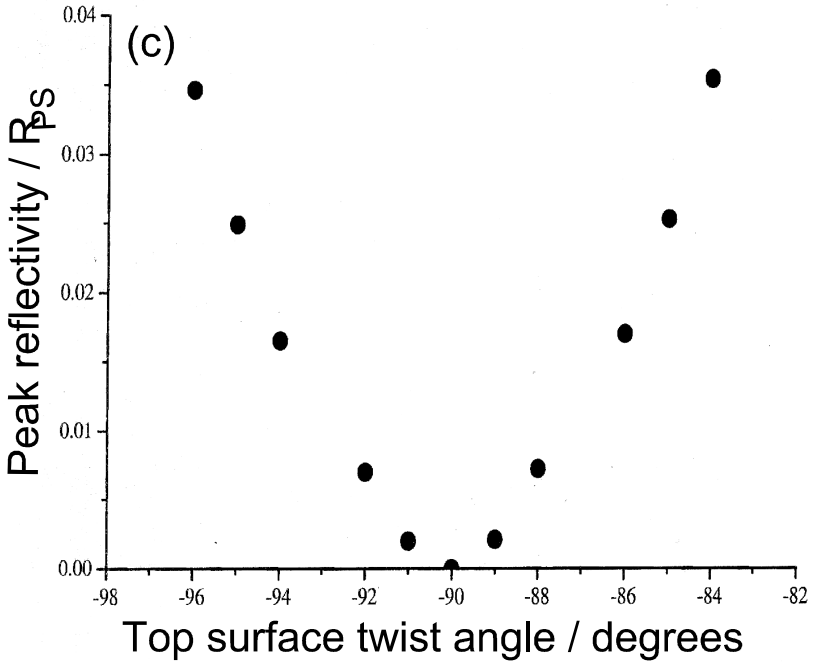

Fig. 16.20(c)

Ch.16 Guided mode ... Fuzi Yang and J R Sambles

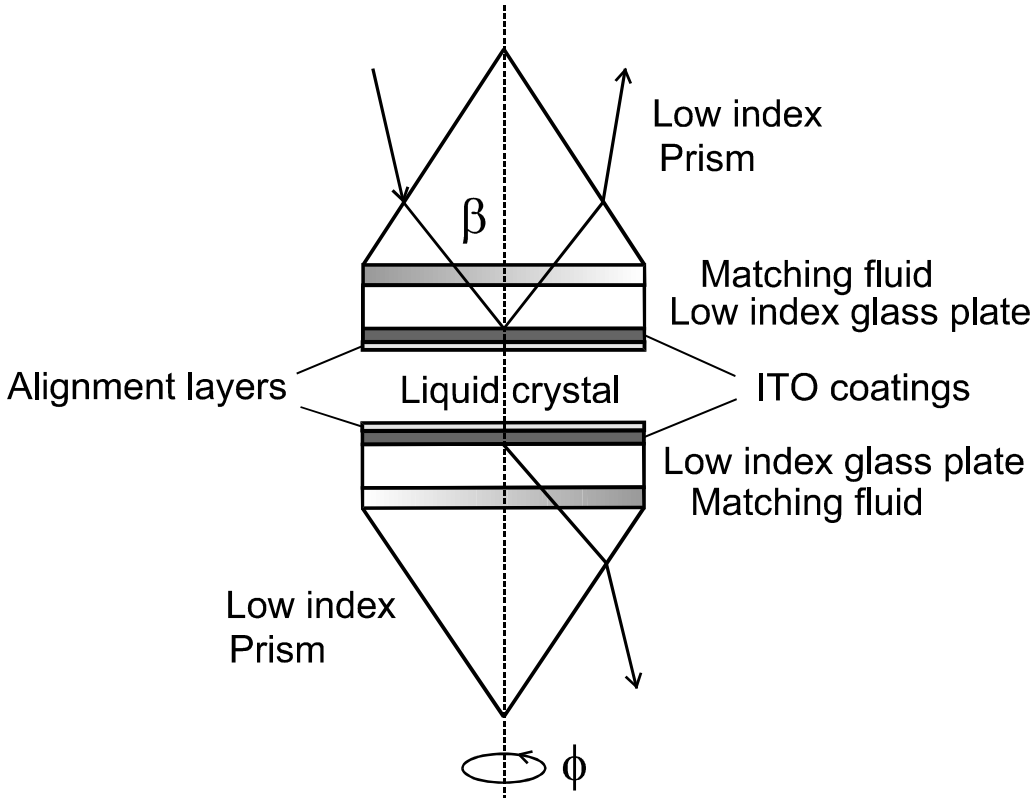

Fig. 16.21

Ch.16 Guided mode ... Fuzi Yang and J R Sambles

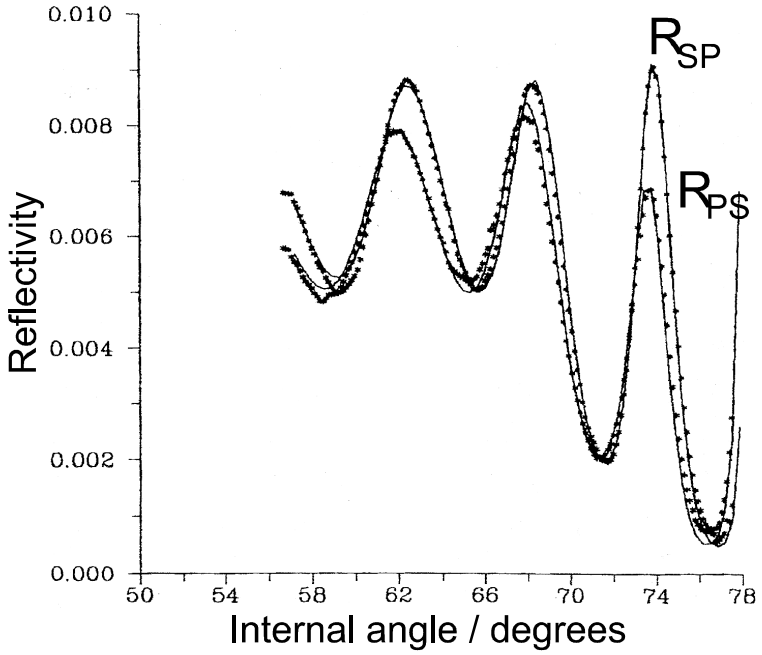

Fig. 16.22

Ch.16 Guided mode ... Fuzi Yang and J R Sambles

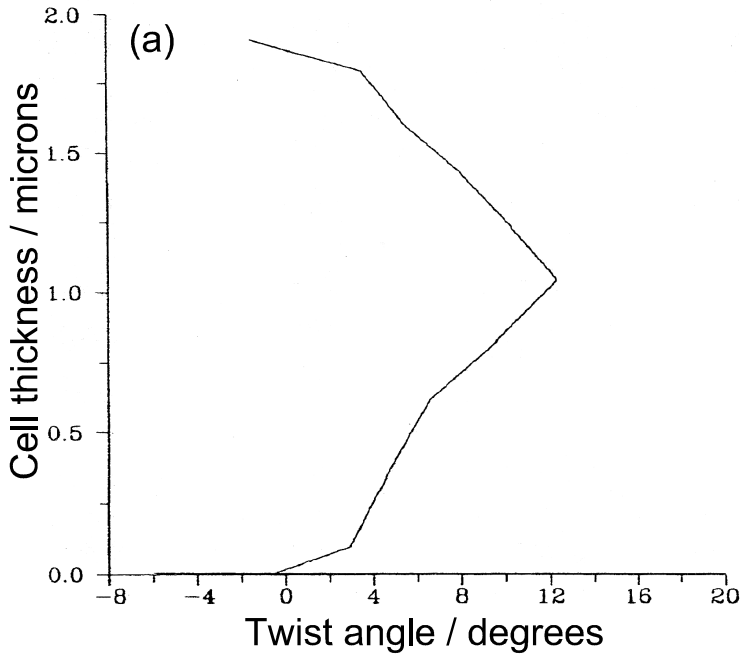

Fig. 16.23(a)

Ch.16 Guided mode ... Fuzi Yang and J R Sambles

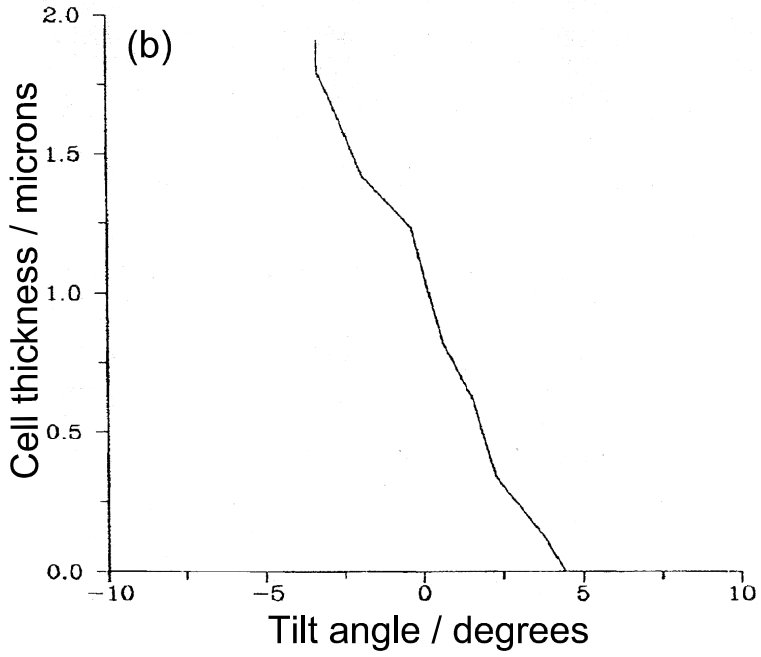

Fig. 16.23(b)

Ch.16 Guided mode ... Fuzi Yang and J R Sambles

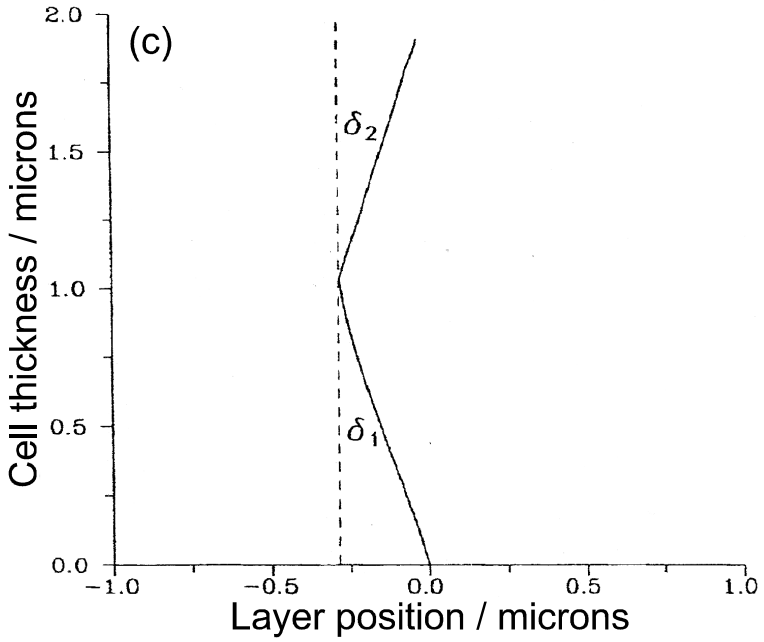

Fig. 16.23(c)

Ch.16 Guided mode ... Fuzi Yang and J R Sambles

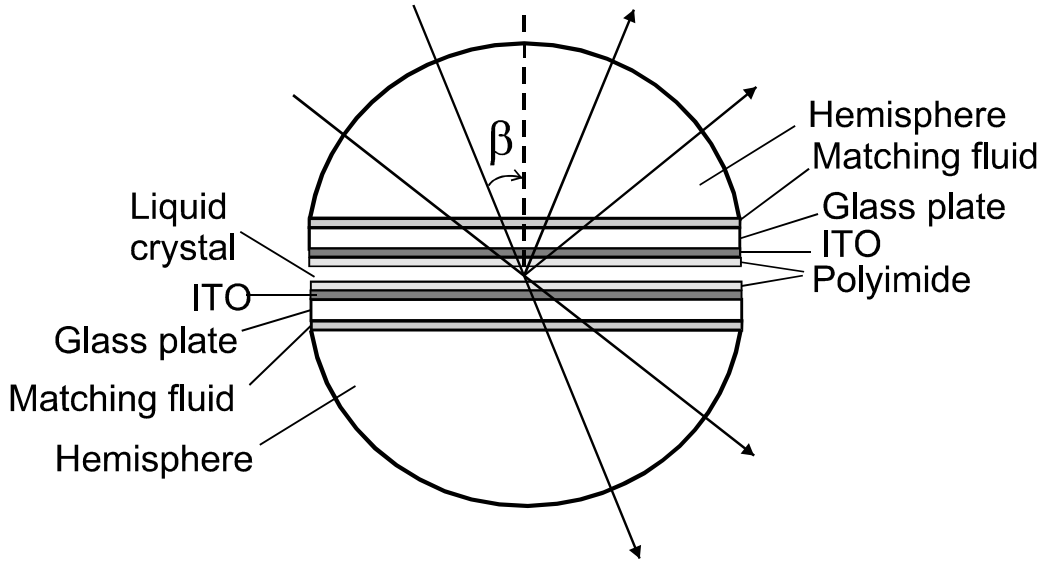

Fig. 16.24

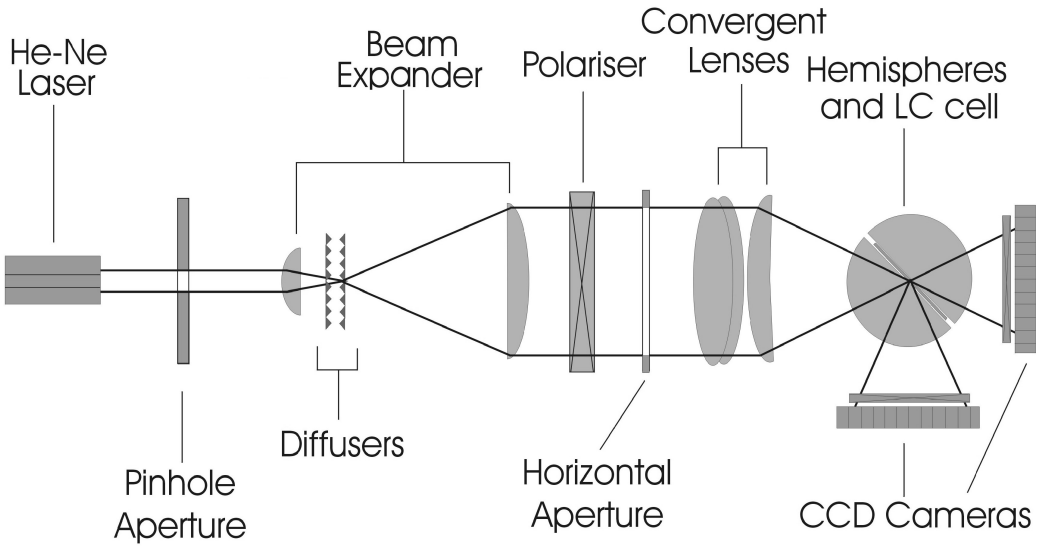
He-Ne
Laser
Beam
Expander
Polariser
Convergent
Lenses
Hemispheres
and LC cell
Pinhole
Aperture
Diffusers
Horizontal
Aperture
CCD Cameras

Fig. 16.25

Ch.16 Guided mode ... Fuzi Yang and J R Sambles

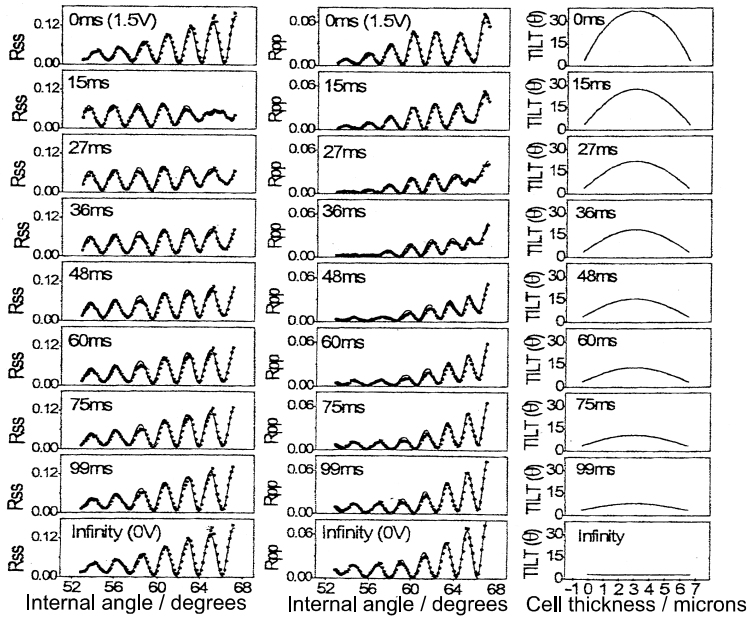

Fig. 16.26